



저작자표시-비영리-변경금지 2.0 대한민국

이용자는 아래의 조건을 따르는 경우에 한하여 자유롭게

- 이 저작물을 복제, 배포, 전송, 전시, 공연 및 방송할 수 있습니다.

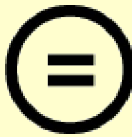
다음과 같은 조건을 따라야 합니다:



저작자표시. 귀하는 원저작자를 표시하여야 합니다.



비영리. 귀하는 이 저작물을 영리 목적으로 이용할 수 없습니다.



변경금지. 귀하는 이 저작물을 개작, 변형 또는 가공할 수 없습니다.

- 귀하는, 이 저작물의 재이용이나 배포의 경우, 이 저작물에 적용된 이용허락조건을 명확하게 나타내어야 합니다.
- 저작권자로부터 별도의 허가를 받으면 이러한 조건들은 적용되지 않습니다.

저작권법에 따른 이용자의 권리는 위의 내용에 의하여 영향을 받지 않습니다.

이것은 [이용허락규약\(Legal Code\)](#)을 이해하기 쉽게 요약한 것입니다.

[Disclaimer](#)

**Thesis for the Degree of Master of Engineering**

**Locomotion Control of a Six-Legged  
Walking Robot Based on Central  
Pattern Generator Network**



by

**Dong Bo Sheng**

**Department of Interdisciplinary Program of  
Mechatronics Engineering**

**The Graduate School**

**Pukyong National University**

**August 2016**

**Locomotion Control of a Six-Legged  
Walking Robot Based on Central  
Pattern Generator Network**

**중심 패턴 발생기 네트워크에 기반한  
6족 보행로봇의 보행제어**

by

**Dong Bo Sheng**

**Advisor: Professor Sang Bong Kim**

**A thesis submitted in partial fulfillment of the requirements for  
the degree of Master of Engineering**

**In the Department of Interdisciplinary Program of  
Mechatronics Engineering,  
The Graduate School,  
Pukyong National University**

**August 2016**

# **Locomotion Control of a Six-Legged Walking Robot Based on Central Pattern Generator Network**

A thesis

by

**Dong Bo Sheng**

Approved as to styles and contents by:

---

(Chairman) **Gi Sik Byun**

---

(Member) **Young Seok Jung**

---

(Member) **Sang Bong Kim**

**May, 2016**

# Acknowledgments

It is a pleasure to express my gratefulness to all the helps and continuous supports from professors, colleagues, family, and friends. First of all, I would like to thank Professor Sang Bong Kim for his valuable advice, guidance, and support since my first days studying and living in CIMEC Lab. His kindness, insight supports and strong motivation encouraged and helped me to accomplish my research and finish this dissertation scientifically. Like other students who had been under his advice, I would like to wish my Professor and his family to have the long-lived health and happiness.

I would like to thank the members of my thesis committee: Prof. Gi Sik Byun, Young Soek Jung who have provided wonderful feedback on my work and great suggestions for better contribution of my dissertation.

I would like to thank Prof. Hak Kyeong Kim for his great helps to research and complete this dissertation. I could not finish my research and dissertation on time without his great help.

I would like to thank all members of CIMEC Lab. for giving me a comfortable and active environment to achieve my work: Dr. Hoang Giang, Dr. Phuc Thinh Doan, Dr. Van Tu Duong, Dr. Pandu Sandi Pramata, Mr. Jung Hu Min, Mr. Jin Wook Kim, Mr. Quang Tuyen Tran, Mr. Yuhanes Dedy Setiawan, Ms. Amuruta Vinod Gulalkari, Mr. Ding Xingkun, Mr. Jeong Jae Hoon, Mr. Husam Hasan, Mr. Nguyen Tron Hai, Mr. Hung Nguyen Huy, Mr. Gao Tianshui and all other foreign friends.

Finally, I would like to thank my grandfather, my grandmother, my father, my mother, my brother, my sister-in-law, my girlfriend and all my close relatives for their love, endless encouragements for me not only in the dissertation time but also in the whole of my life. And lastly, thanks for all the people who cannot be mentioned here for their help and support.

Pukyong National University, Pusan, Korea

June 1, 2016



Dong Bo Sheng



# Contents

<b>Acknowledgement</b> .....	<b>i</b>
<b>Contents</b> .....	<b>iii</b>
<b>Abstract</b> .....	<b>vi</b>
<b>List of Figures</b> .....	<b>viii</b>
<b>List of Tables</b> .....	<b>xi</b>
<b>Nomenclature</b> .....	<b>xii</b>
<b>Chapter 1: Introduction</b> .....	<b>1</b>
1.1 Background and motivation.....	1
1.2 Problems statements.....	7
1.3 Objective and research method.....	8
1.4 Outline of thesis and summary of contributions .....	9
<b>Chapter 2: System Description and Kinematic Modeling</b> .....	<b>12</b>
2.1 Mechanical design.....	12
2.2 Electrical design .....	14
2.2.1 Microcontroller .....	15
2.2.2 Servomotors .....	16
2.2.3 Bluetooth.....	19
2.2.4 MySen-M sensor .....	20
2.2.5 Power supply.....	21
2.3 Basic terminologies of the 6LR.....	21
2.4 Kinematic modeling of four joint legs .....	27

2.5 Kinematics of the six legged robot.....	30
<b>Chapter 3: CPG Model and Parameters Analysis .....</b>	<b>35</b>
3.1 CPG model.....	35
3.2 Parameters analysis .....	38
3.2.1 Parameter $u_0$ .....	39
3.2.2 Parameter $\beta$ .....	40
3.2.3 Parameter $w_{fe}$ .....	41
3.2.4 Parameter $\tau$ .....	42
3.2.5 Parameter $\tau'$ .....	43
<b>Chapter 4: Gait Planning Based on CPG Network and Controller</b>	
<b>Design .....</b>	<b>45</b>
4.1 CPG network.....	45
4.1.1 Wave gait .....	46
4.1.2 Quadruped gait.....	48
4.1.3 Tripod gait.....	50
4.2 Mapping function.....	52
4.3 Workspace trajectory tracking controller design .....	55
<b>Chapter 5: Simulation and Experimental Results .....</b>	<b>62</b>
5.1 Gait planning simulation results.....	62
5.1.1 Wave gait .....	63
5.1.2 Quadruped gait.....	64
5.1.3 Tripod gait.....	65

5.2 Mapping function of tripod gait simulation results.....66

5.3 Workspace trajectory tracking .....69

**Chapter 6: Conclusions and Future Work .....74**

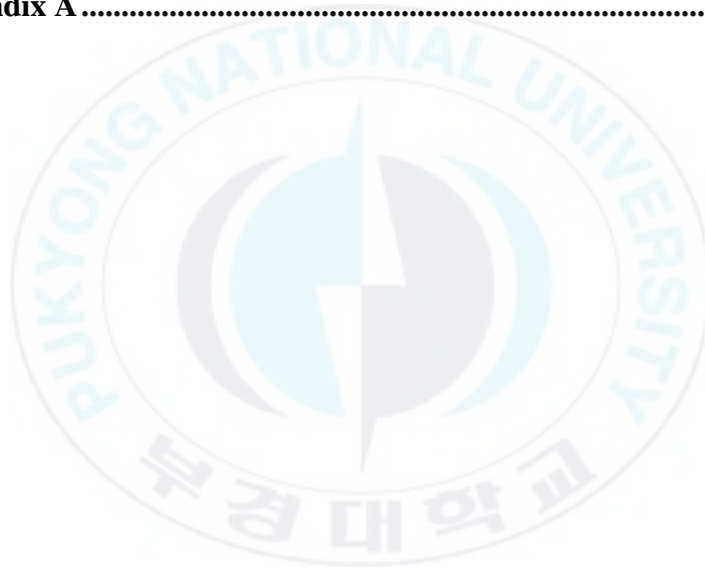
6.1 Conclusions .....74

6.2 Future work .....76

**References .....77**

**Publication and Conferences .....83**

**Appendix A .....85**



# **Locomotion Control of a Six-Legged Walking Robot Based on Central Pattern Generator Network**

**Dong Bo Sheng**

**Department of Interdisciplinary Program of  
Mechatronics Engineering,  
The Graduate School, Pukyong National University**

## **Abstract**

In recent years, much attention has been given to bionic control. The motion control of legged robots based on central pattern generator (CPG) has become one of the important branches of bionic control field as a research hotspot. CPG can produce steady rhythm without any high-level external control signal and sensory feedback, which does not require the model process on environment.

The objective of this thesis is to control the locomotion of a six-legged walking robot based on central pattern generator network. To do this task, the following problems are considered. Firstly, a six-legged walking robot is presented. Secondly, wave gait, quadruped gait and tripod gait should be generated by CPG network. Thirdly, mapping function is designed to map the output signal of CPG network to the workspace trajectories of the corresponding legs. Fourthly, instead of using inverse kinematics to calculate joint angles, a differential kinematics algorithm is applied for the end effector to follow the trajectory generated by CPG network. The following tasks

are done to solve these problems. First, a six legged robot platform is developed with several interconnected devices such as AX-12 servomotor, DSP microcontroller, IMU sensor, etc. The kinematics of one leg of the six-legged robot is presented, and the Denavit-Hartenberg (DH) convention is adopted to define the modeling parameters which allow the construction of the forward kinematics function by composition of the individual coordinate transformation. Second, a CPG model based on Kimura's neural oscillators is proposed. To get a suitable control signal of CPG, the parameters of CPG model are analyzed based on a single-parameter-analysis method using simulation. Third, a CPG network to generate control signal for wave gait, quadruped gait and tripod gait using six CPG models is built. Fourth, mapping functions to change the control signal of CPG into the workspace trajectory are proposed. For swing phase and retract phase of gait, different mapping functions are used. The end effector trajectory of each leg is given as mapping functions of the output of signal of the corresponding oscillator. Fifth, to realize the leg end effector follow the trajectory obtained by the mapping functions, a differential kinematics algorithm is applied to solve inverse kinematics problem easily, and the differential kinematics is represented as a linear mapping between the joint velocity space and the operational velocity space. Finally, simulation and experimental results are done to demonstrate the effectiveness of the proposed controllers.

**Keywords:** Central pattern generator (CPG), CPG network, Mapping function, Six-legged robot, Differential kinematics.

# List of Figures

Fig. 1.1 Genghis walking robot.....	2
Fig. 1.2 Hannibal and Attila walking robot .....	2
Fig. 1.3 BigDog walking robot .....	3
Fig. 1.4 Underwater robot Crabster CR200 .....	3
Fig. 1.5 Quadruped walking robot Tekken .....	5
Fig. 1.6 Multi-legged robot: NEXUS .....	6
Fig. 2.1 System configuration of 6LR. ....	13
Fig. 2.2 Real 6LR.....	13
Fig. 2.3 One leg configuration .....	14
Fig. 2.4 Control system structure of the 6LR.....	15
Fig. 2.5 DSP TMS320F28335 .....	16
Fig. 2.6 Dynamixel AX-12A .....	16
Fig. 2.7 Half duplex UART circuit .....	17
Fig. 2.8 Touch detection method .....	18
Fig. 2.9 Bluetooth Promi SD202.....	19
Fig. 2.10 mySen-M sensor .....	20
Fig. 2.11 12V battery ATLASBX ITX100 .....	21
Fig. 2.12 Leg cycle of one leg.....	22
Fig. 2.13 Support polygon of the 6LR .....	23
Fig. 2.14 Front end rear margins.....	24
Fig. 2.15 Statically unstable gait.....	25
Fig. 2.16 Workspace of one leg .....	26
Fig. 2.17 Swing phase of step cycle of leg $i$ .....	26
Fig. 2.18 Retract phase of step cycle of leg $i$ .....	27
Fig. 2.19 Configuration of one leg.....	28

Fig. 2.20 Frame coordinates of the 6LR .....	31
Fig. 3.1 Neural oscillator as a model of CPG .....	37
Fig. 3.2 Output of CPG according to $u_0$ value .....	40
Fig. 3.3 Output of CPG according to $\beta$ value .....	41
Fig. 3.4 Output of CPG according to $w_{fe}$ value .....	42
Fig. 3.5 Output of CPG according to $\tau$ value .....	43
Fig. 3.6 Output of CPG according to $\tau'$ value .....	44
Fig. 4.1 CPG network of the six-legged walking robot .....	46
Fig. 4.2 Walking cycle of the wave gait .....	47
Fig. 4.3 Each state time in one cycle time of the wave gait.....	47
Fig. 4.4 Topology of CPG network for wave gait .....	48
Fig. 4.5 Walking cycle of the quadruped gait.....	49
Fig. 4.6 Each state time in one cycle time of the quadruped gait .....	49
Fig. 4.7 Topology of CPG network for quadruped gait.....	50
Fig. 4.8 Walking cycle of the tripod gait .....	51
Fig. 4.9 Each state time in one cycle time of the tripod gait.....	51
Fig. 4.10 Topology of CPG network for tripod gait .....	52
Fig. 4.11 End effector trajectory of one leg of the 6LR.....	53
Fig. 4.12 End effector position control of leg $i$ .....	56
Fig. 4.13 Block diagram of workspace trajectory tracking controller .....	61
Fig. 5.1 Output of CPG network for wave gait.....	64
Fig. 5.2 Output of CPG network for quadruped gait .....	65
Fig. 5.3 Output of CPG network for tripod gait.....	66
Fig. 5.4 One cycle of CPG network output for tripod gait .....	67
Fig. 5.5 Transformed trajectory for $y$ axis.....	68
Fig. 5.6 Transformed trajectory for $z$ axis.....	68

Fig. 5.7 The end effector of one leg at stand position.....70

Fig. 5.8 Tracking errors of the end effector of one leg for one walking cycle time .....71

Fig. 5.9 Joint angular velocity of one leg of the six-legged robot for one walking cycle time .....71

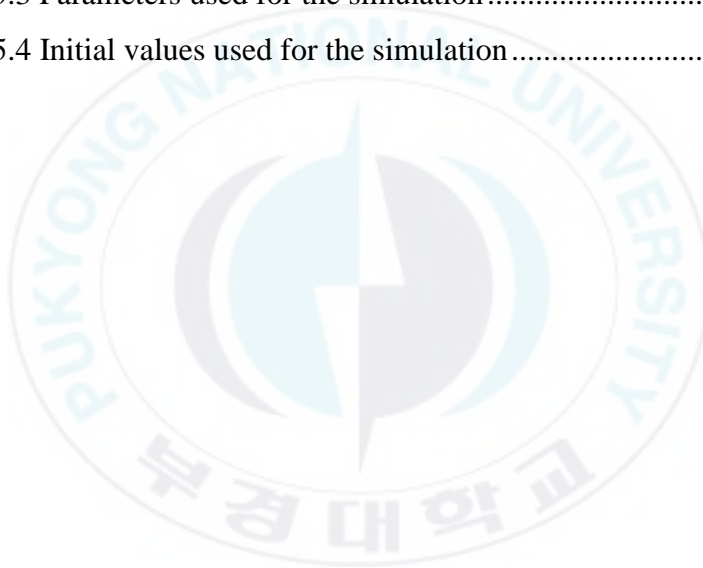
Fig. 5.10 Joint angles of one leg of the six-legged robot for one walking cycle time .....72

Fig. 5.11 Trajectory of end effect of one leg of one walking cycle time .....73



## List of Tables

Table 2.1 Specification of Dynamixel AX-12A actuator .....	17
Table 2.2 Specification of Bluetooth Promi SD202 .....	20
Table 2.3 Specification of 12V battery ATLASBX ITX100.....	21
Table 2.4 D-H parameters of 4-Link leg.....	29
Table 5.1 Values of the parameters of the CPG network .....	62
Table 5.2 Parameters used for the simulation.....	66
Table 5.3 Parameters used for the simulation.....	69
Table 5.4 Initial values used for the simulation.....	69



# Nomenclatures

Variables	Descriptions	Units
$T$	Leg cycle time	s
$T_{sw}$	Swing phase time	s
$T_{rt}$	Retract phase time	s
$\rho$	Duty factor	s
$R$	Stroke length	m
$h$	Height of working space of one leg	m
$r$	Distance of one step	m
$O_{ji}$	Origin of the joint $j$ of leg $i$	
$\theta_{ji}$	Rotational angle of joint $j$ of leg $i$	rad
$\alpha_i$	Denavit-Hartenberg convention parameters	rad
${}^j_k T_i$	Transformation matrix from joint $j$ coordinate system to joint $k$ coordinate system of leg $i$	
$k(\theta_i)$	Forward kinematic function	
$E$	Distance between two front legs (or two rear legs)	m
$L$	Length of the 6LR	m
$W$	Distance between two middle legs	m
$\beta$	Orientation angle	rad
$\mathbf{p}_{ei}^b$	End effector position vector of leg $i$ with respect to body frame	
$\mathbf{p}_{di}^b$	Desired end effector position vector of leg $i$ with respect to body frame	
$\mathbf{e}_i^b$	End effector position error vector of leg $i$	

$\mathbf{J}_{Ai}^b(\boldsymbol{\theta}_i)$	Analytical Jacobian of $\mathbf{p}_{ei}^b$ with respect to $\boldsymbol{\theta}_i$
$V_i(\mathbf{e}_i^b)$	Candidate Lyapunov function of leg $i$
$\omega(\boldsymbol{\theta}_i)$	Objective function of joint variables of leg $i$
$\dot{\mathbf{q}}_{0i}$	Additional vector for constraint of joint configuration of leg $i$
$(\mathbf{J}_{Ai}^b)^+$	Right pseudo-inverse of $\mathbf{J}_{Ai}^b$ of leg $i$
$\tau_{1i}$	Torque implied on joint 1 of leg $i$
$\mathbf{p}_{0i}^b$	Default standing position vector of leg $i$
$\mathbf{p}_{AEPi}^b$	Anterior Extreme Position (AEP) vector of leg $i$
$\tau$	Time constant of $u_{\{e,f\}i}$
$\tau'$	Time constant of $v_{\{e,f\}i}$
$y_{ei}$	The output of extensor oscillator
$y_{fi}$	The output of flexor oscillator
$w_{fe}$	Connection weight between flexor and extensor oscillator
$\beta$	Constant representing the degree of the self-inhibition influence on the inner state
$u_0$	External input with a constant rate
$feed_{\{e,f\}i}$	A feedback signal
$k_z$	The amplitude gain coefficients

# Chapter 1: Introduction

## 1.1 Background and motivation

With the development of science and technology, robots are used in many fields such as military transport and exploration, submerged structure, submarine detection, planetary exploration and so on. A walking legged robot can adapt to the complex and changeable environment because of its multiple degrees of freedom (DoF), discontinuous ground walking with attitude stability and omnidirectional walking ability [1].

Because the walking legged robot is a complex system with multivariable parameters, strong coupling and nonlinear structural dynamics, controlling the locomotion of the walking legged robot is more difficult than that of a mobile robot. To control the locomotion of walking legged robot, manual planning combined with other control theory always be used. There are several defects with using manual planning method such as complex measurement and calculation, poor real-time performance, complex locomotion control algorithm with the increase of the number of controlled parameters and lack of flexibility and autonomy. In the walking legged robot, a six-legged robot (6LR) is the most common legged robot since its structure is more stable than a bipedal robot or a quadruped robot [2].

In 1989, Brooks proposed a new architecture for controlling a six legged walking robot capable of walking over rough terrain and following a person passively sensed in the infrared spectrum named Genghis shown as Fig. 1.1 [3]. Each leg had two DC motors. So each

leg had two degree of freedom. Also the robot equipped two single axis accelerators and two touch sensors for walking over rough terrain with attitude stability.



Fig. 1.1 Genghis walking robot

In 1990, another six-legged robot were built in the Mobot Lab named Attila and Hannibal shown as Fig. 1.2. They were recognized as being among the most sophisticated autonomous robots for their size, possessing over 19 degrees of freedom, over 60 sensory inputs, and over 8 microprocessors [4]. However, the system was too complex.

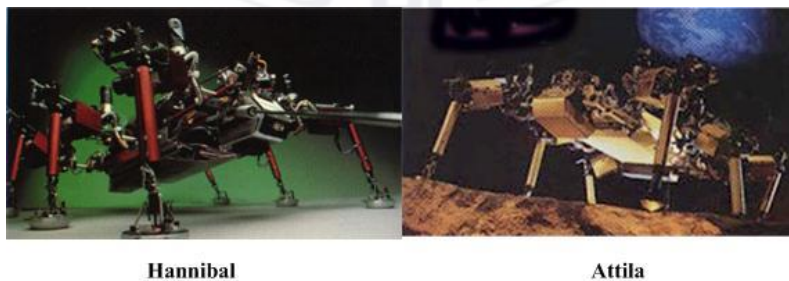


Fig. 1.2 Hannibal and Attila walking robot

M. Raibert and his colleagues created an animal-like robot with advanced behavior named BigDog shown as Fig. 1.3 [5]. This robot

could move up to 4 mph on very hard terrains, to climb slopes up to 35 degrees and to carry a load of 150kg. However the robot was too heavy and the locomotion control system was too complex.



Fig. 1.3 BigDog walking robot

In 2014, Korean Research Institute of Ships and Science and Ocean Engineering (KRIOS) developed an underwater robot capable of conducting dangerous undersea exploration named Crabster CR200 shown as Fig. 1.4 [6]. The dimensions, joint structure, range of motion and mass distribution of the robot were determined by considering biological data, and then suitable joint actuators were chosen through a simple force analysis.



Fig. 1.4 Underwater robot Crabster CR200

There are several researches focusing on locomotion control of the walking legged robot. One of the locomotion control methods of the walking legged robot is based on modeling-planning-controlling. First, modeling of the walking legged robot and environment is built. Second, the optimal trajectory of locomotion is got by manual planning. Third, by decreasing the error between current position and optimal trajectory, make the robot following the optimal trajectory.

Recently, locomotion control for a legged robot based on biologic concepts has been a new research area. In 1966, M. L. Shik et al. proposed the rhythmic motion was controlled by central pattern generator (CPG) [7]. In nature, the rhythmic motion was the most usual locomotion such as walking, running, swimming, etc. Locomotion control based on central pattern generator (CPG) was an important branches of bionic control, and biologically inspired method have been adopted to control legged robot [8-9]. Central pattern generator consists of a few neuron oscillators that produce stable rhythmic patterned output without higher-level command or sensory feedback, and higher-level command and sensory feedback also can make CPG regulation and stability [10-12].

In 1980, Cohen proposed the first CPG model through the research on the dissection of a lamprey spinal cord [13]. Matsuoka proposed a neural rhythm generator model in 1985, and this model solved the problem of only one neural oscillator [14]. By adapting the weight between neural oscillators, the output of CPG also could be changed. However, the higher-level command and the sensory feedback were not attached, so complex motion control is difficult to achieve. In 1997, S. T. Venkataraman applied CPG to achieve gait

planning and control of a hexapod insect robot. However, the motion achieved is simple [15]. Taga changed the constant input continuously to realize the transition from walking to running in a biped robot model [16]. Billard et al. used the same approach in Sony's dog, AIBO, to transit from walking to trotting and galloping [17]. Kimura et al. achieved locomotion control of a quadruped robot walking on irregular terrain based on CPG [18-19]. By using visual sensor information and simple adjustments of reflexes, adaptive dynamic walking on irregular terrain was realized. Y. Fukuoka et al. applied CPG on the quadruped walking robot named Tekken as shown in Fig. 1.5 [20]. However, the response mode was single, and could not respond to any kind of incentives and change the motion by higher-level, also one CPG only could control one joint. P. Manoonpong et al. achieved high level behaviors in his research such as reflex and escape based on sensor-driven neural control [21]. His robot could walk omnidirectionally but with only tripod gait.

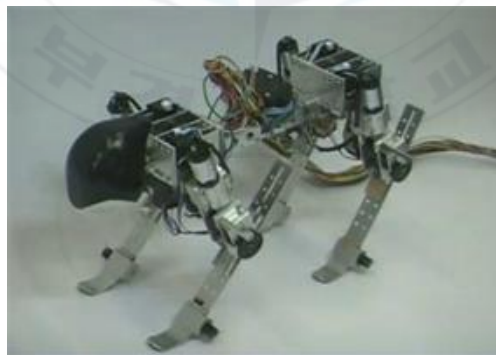


Fig. 1.5 Quadruped walking robot Tekken

Inspired by lamprey's swimming CPG, A. J. Ijspeert et al. have researched the motion of salamander and snake robots. In their research, one CPG unit was used to control one degree of freedom,

and a distributed CPG network could generate complex coordinated multidimensional output signals to realize the swimming or serpentine locomotion[22-25]. For some crawling robots, joint control signals are simple to achieve. For legged robot, such as a quadruped robot or a six-legged robot, joint control space are more complex. The stability of a walking robot is usually realized by adjusting parameters of CPG model to generate coordinated joint control signals. For a six-legged robot, many neural oscillators are required to control the multi-degree of freedom, and it's difficult to adjust too many parameters to obtain required output signals.

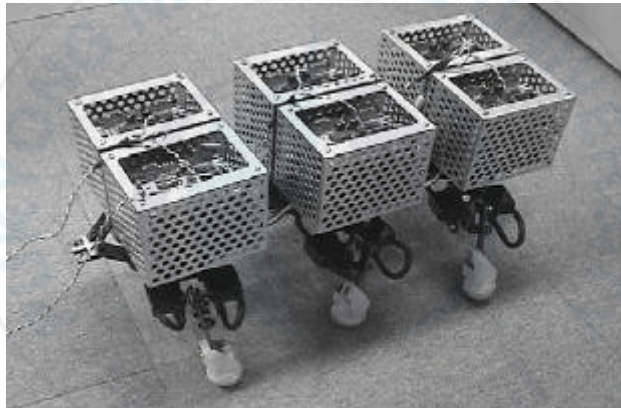


Fig. 1.6 Multi-legged robot: NEXUS

S. Inagaki et al. proposed gait-pattern generation mechanism and walking speed control of an autonomous decentralized multi-legged robot system shown as Fig. 1.6 [26-27]. The CPG model can generate oscillation patterns depending only on the network topology and can bifurcate different oscillation patterns according to the network energy.

In 2001, K. Tsuchiya et al. proposed a control system for locomotion of a legged robot based on CPG, and realized stable locomotion for a quadruped robot and a ten-legged locomotion robot [28]. In [29], a controller composed of a leg motion controllers and a gait pattern controller was proposed. The leg motion controller drove all the joint actuators of the legs so as to realize the desired motion generated by the gait pattern controller. In [30], Endo et al. had explored a locomotion control method in the task space of a legged robot.

## **1.2 Problems statement**

There are few researches for applying the CPG for locomotion control of six-legged robot. To control locomotion of the six-legged robot using CPG is not an easy task, and there also exist some problems to do so as follows:

- (1) Some CPG models are complex, lead control system to be more complex.
- (2) It's difficult to tune the parameter of CPG model
- (3) One CPG model is used to control one joint. For controlling a six-legged robot, lots of CPG models must be used. Therefore, it makes the CPG network be complex.
- (4) For the legged robot, by mapping CPG signals to joint control signals is difficult to achieve adaptive locomotion control by changing the parameters of CPG model.
- (5) The inverse kinematics problems is the determination of joint angles corresponding to a given end effector position. However, the equations of the inverse kinematics are

nonlinear, and it is not always possible to find their solution, and there may exist multiple solutions.

### **1.3 Objective and research method**

To solve the problems mentioned in the above discussions, the objective of this thesis is to control the locomotion of a six-legged walking robot based on central pattern generator. To do this task, Firstly, a six-legged walking robot is prepared. Secondly, wave gait, quadruped gait and tripod gait should be generated by CPG network. Thirdly, mapping functions are designed to map the output signal of CPG network to the workspace trajectories of the corresponding legs. Fourthly, instead of using inverse kinematics to calculate joint angular, a differential kinematics algorithm is applied for the end effector to follow the trajectory generated by CPG network, and the simulation and experiment to evaluate the controller are done

The locomotion control of 6LR is divided into gait planning and attitude stabilizing control. For gait planning, a central pattern generator model based on Matsuoka's oscillator is used. To get the desired phase signal, the parameters of CPG model is analyzed by a single-parameter-analysis method.

To obtain the different gaits of 6LR, a CPG network is built by using six coupled neural oscillators. Three kinds of phase signal to generate three kinds of gaits are obtained by using different connecting weight between six coupled neural oscillators such as wave gait, quadruped gait and tripod gait. Mapping functions to

convert the phase signal generated by CPG network to workspace trajectory of end effector of each leg is designed.

The inverse kinematics problem is the determination of the joint angle corresponding to a given end effector position. Instead of using inverse kinematics to calculate joint angular, differential kinematics algorithm is applied for the end effector to follow the trajectory generated by CPG network.

Finally, the simulation and experimental results of walking on the slop plane are presented to verify the effectiveness of the proposed controllers.

#### **1.4 Outline of thesis and summary of contributions**

This section describes the contents of the thesis and its contributions briefly. The contents consist of seven sections as follows:

##### **Chapter 1: Introduction**

In this chapter, background and motivation of this thesis are presented. Problem statement of this research are given. Objective and research method of this thesis are then described. Finally, outline and summary of contribution of this thesis are given.

##### **Chapter 2: System Description and Kinematic Modeling**

In this chapter, the description of a six-legged robot and its hardware configuration are presented, and the typical

definitions for the six-legged robot and the stability of walking gait are stated. The kinematic modeling of one leg of the six-legged robot is presented based on D-H convention.

### **Chapter 3: Neural Oscillator Model and Parameters Analysis**

This chapter describes the CPG model based on Kimura's neural oscillator model, which corresponds to flexor neural and extensor neuron, respectively. The parameters analysis of the CPG model is presented.

### **Chapter 4: Gait Planning Based on CPG Network and Controller Design**

This chapter describes a CPG network to generate three kinds of gait for the six-legged walking robot such as wave gait, quadruped gait and tripod gait. Six coupled oscillators are used to denote the CPG network, and each oscillator is used to control one leg by generate phase signal. Gait transition by changing the connecting weight matrix is achieved. Mapping functions are designed to map the phase signals generated by CPG network to the workspace trajectory of the corresponding end effector of legs. And a workspace trajectory tracking controller design to control the leg end effector of one leg to track the trajectory generated by mapped the output signal of CPG network based on differential kinematics algorithm.

### **Chapter 5: Simulation and Experimental Results**

This chapter presents simulation and experimental results of the proposed controllers. The simulation and experimental results of walking on the slop plane are presented to verify the effectiveness of the proposed controllers.

## **Chapter 6: Conclusions and Future Works**

Conclusions from this research and some ideas for future works are presented.



## **Chapter 2: System Description and Kinematic Modeling**

This chapter describes the prototype of six-legged robot (6LR) system and basic terminologies of the 6LR. The robot developed in this thesis consists of mechanical design, electrical design. The mechanical design is comprised of a body and six legs. The electrical design consists of motors, microcontroller, host computer and power supply.

### **2.1 Mechanical design**

The configuration of 6LR system used for this thesis is shown in Fig. 2.1. The 6LR developed in this thesis consists of one body and six legs such that each leg has four rotational joints and four links. For the simplicity of symbols, six legs are numbered as 1, 2, 3 for Leg-L1, Leg-L2, Leg-L3 and 4, 5, 6 for Leg-R3, Leg-R2, Leg-R1. The microcontroller and Bluetooth are attached on the inner side of the body frame of 6LR to control the servomotors and to communicate with the host computer, respectively.

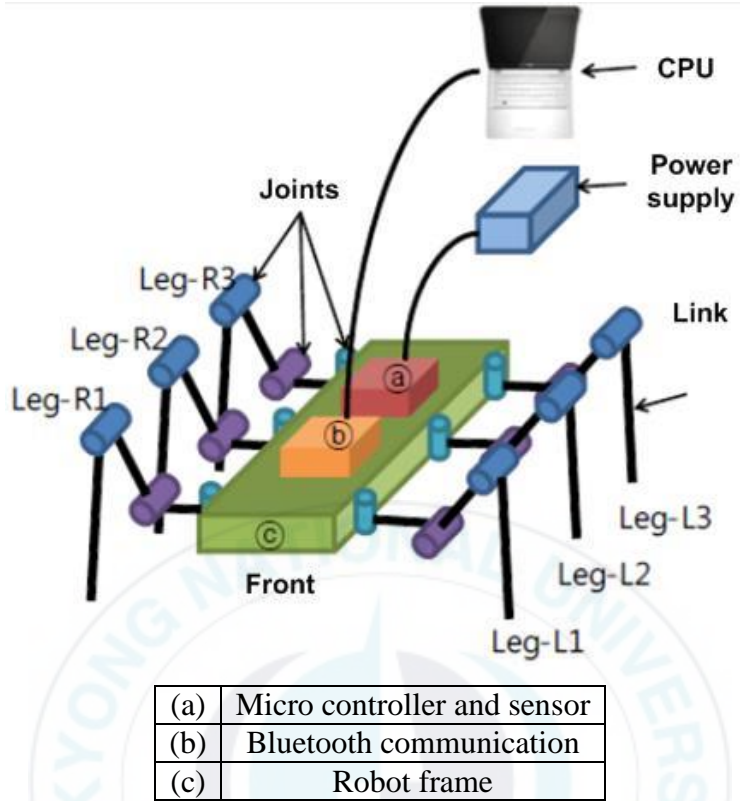


Fig. 2.1 System configuration of 6LR

The real Kinect camera based 6LR system developed for this thesis is shown in Fig. 2.2.

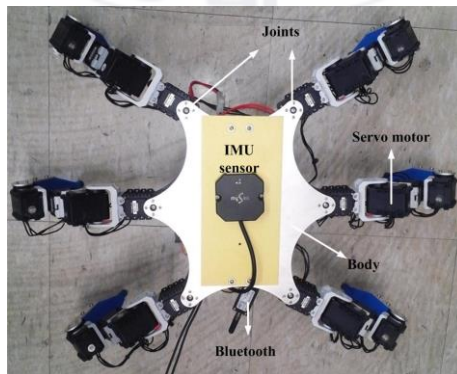


Fig. 2.2 Real 6LR

For the leg configuration, there are 24 servo motors used to control the locomotion of 6LR by operating 6 legs (i.e., 24 rotational joints). Each leg has four rotational joints, four links and one end effector to touch the ground. This design of legs can make the robot get more complex postures and better stability. Fig. 2.3 shows one leg configuration of 6LR with four rotational joints, four links and end effector.

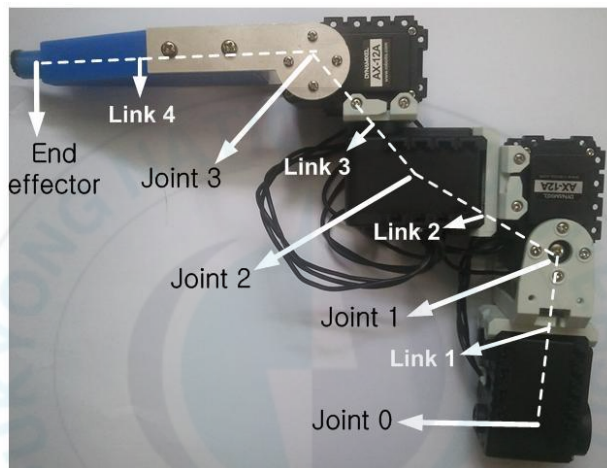


Fig. 2.3 One leg configuration

## 2.2 Electrical design

The electrical configuration of 6LR system is shown in Fig. 2.4. The robot is controlled by host computer and microcontroller. The microcontroller controls all servomotors and receives feedback data from servomotors through half-duplex community. The following sections describe these components with detailed specifications and figures.

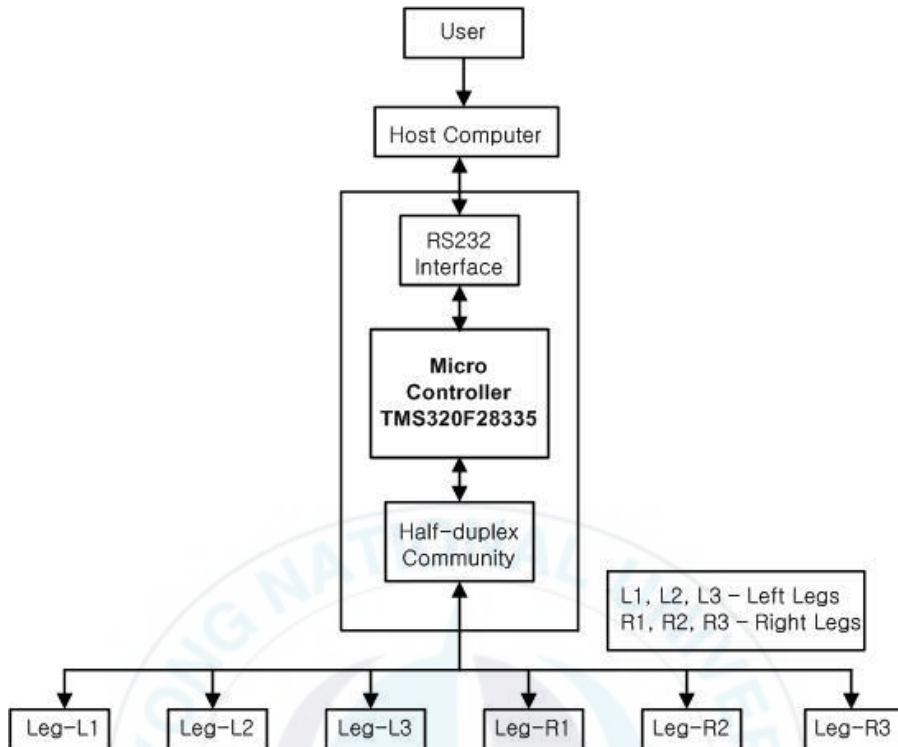


Fig. 2.4 Control system structure of the 6LR

### 2.2.1 Microcontroller

In this thesis, a microcontroller used to control the 6LR is DSP (Digital signal processor) TMS320F28334 shown in Fig. 2.5. This controller sends joint angles calculated by the host computer to the servomotors of each leg, and receives feedback data from the servomotors.



Fig. 2.5 DSP TMS320F28335

### 2.2.2 Servomotors

Servomotors used in this thesis are Dynamixel AX-12A which is shown in Fig. 2.6. The dynamixel series servomotor is a smart, modular actuator that incorporates a gear reducer, a precision DC motor and a circuitry with network functionality. Despite its compact size, it can produce high torque and is made with high quality material to provide the necessary strength and structural resilience to withstand large external forces. The specifications of Dynamixel AX-12A servomotor are listed in Table 2.1.



Fig. 2.6 Dynamixel AX-12A

Table 2.1 Specifications of Dynamixel AX-12A actuator

No.	Parameters	Values
1	Weight (g)	54.6
2	Dimension (W x L x H) (mm)	32 x 50 x 40
3	Resolution (degree)	0.29
4	Gear reduction ratio	254:1
5	Torque (N.m)	1.5
6	No load speed (rpm)	59
7	Running Degree (degree)	0~300
8	Operating temperature (°C)	-5~70
9	Voltage range (V)	9~12
10	Communication speed (bps)	7343~10 <sup>6</sup>
11	Material	Engineering plastic

6LR have six legs and each leg has four joints. There are 24 servomotors to control six legs. To control the dynamixel actuators, the main controller needs to convert its UART signals to the half duplex type. Its recommended circuit diagram is shown in Fig. 2.7. The protocol used by Dynamixel AX-12A is Half Duplex Asynchronous Serial Communication (8bit, 1stop, No Parity).

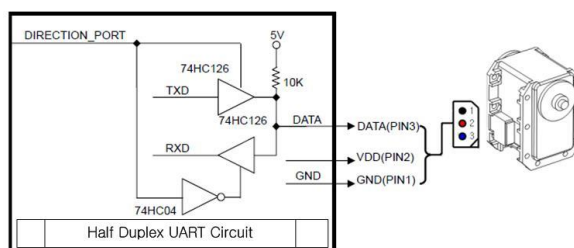


Fig. 2.7 Half duplex UART circuit

The servomotor also has the ability to detect the direction of torque on the motor which can be used as touch detector on joint 1 of each leg. Touch detector is installed at Dynamixel AX-12 servomotor. This kind of servomotor provides data of torque on the actuator. The data are not accurate. They are used only to detect the direction of the torque  $\tau_{1i}$ . Touch detecting method is applied on joint 1 of each leg as shown in Fig. 2.8.  $\tau_{1i}$  is the torque of joint 1 of leg  $i$  ( $i = 1, 2, 3, 4, 5, 6$ ).

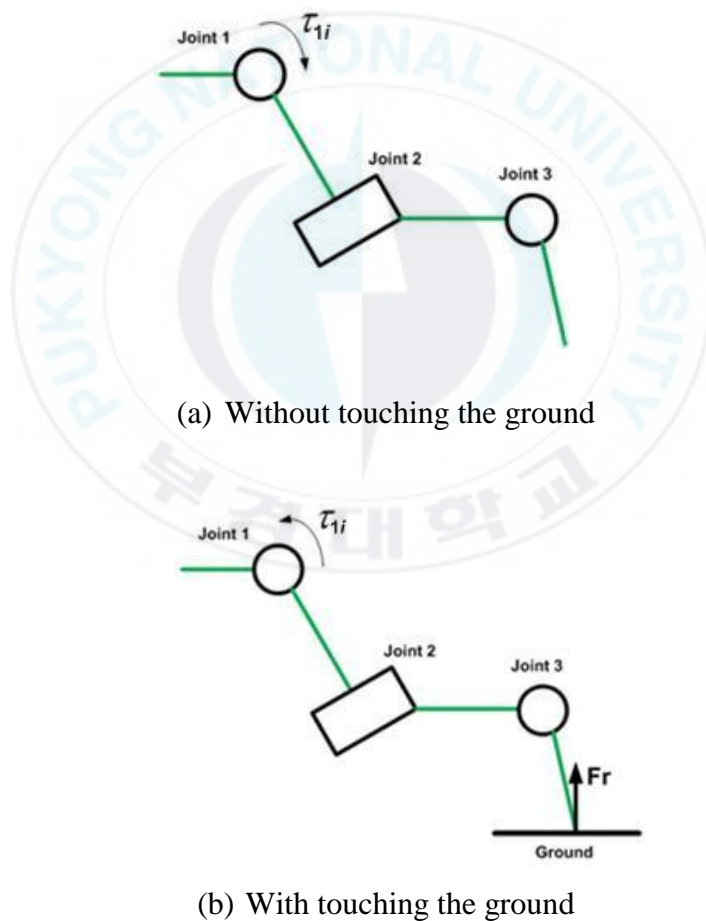


Fig. 2.8 Touch detection method

When the leg doesn't touch the ground, the masses of joints 2 and 3 will make the load on joint 1 negative. When the leg touch the ground, the reaction force  $\mathbf{F}_r$  exert on end effector and make the load on joint 1 positive.

### 2.2.3 Bluetooth

In this thesis, Bluetooth Promi SD202 is used as a wireless communication between 6LR and the host computer. The host computer sends control commands to the DSP microcontroller through this wireless device shown in Fig. 2.9. Table 2.2 shows the specifications of Bluetooth Promi SD202 device.

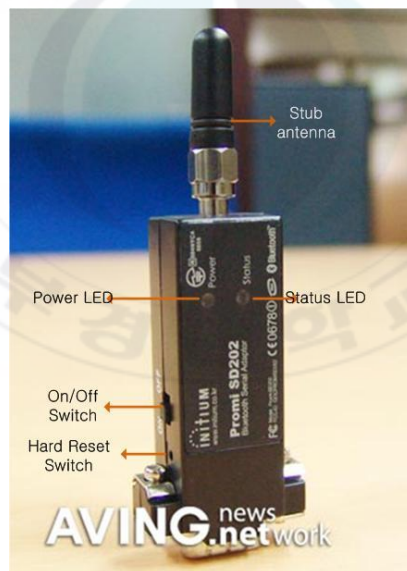


Fig. 2.9 Bluetooth Promi SD202

Table 2.2 Specifications of Bluetooth Promi SD202

No.	Parameters	Values
1	Range (m)	~100
2	Range of baud rate (bps)	1200-230400
3	Supply voltage (V)	4~12
4	Supply current (mA)	150
5	Dimension (mm)	60 x 26 x 16
6	Operating temperature (°C)	-20~70
7	Level(dBm)	18
8	Bluetooth protocols	RFCOMM, L2CAP, SDP
9	Output power (mW)	63

#### 2.2.4 MySen-M sensor

The mySen-M sensor is used to measure the robot angles and its specification are shown in Fig. 2.10.



Static Accuracy	Roll, Pitch	$\leq 1\text{deg}$
	Heading(Yaw)	$\leq 2\text{deg}$
Angular Resolution		0.1deg
Update Rate		100Hz

Fig. 2.10 mySen-M sensor

### 2.2.5 Power supply

In the Kinect camera based 6LR system, voltage requirement for all motors is 9V~12V. Therefore, ATLASBX ITX100 12V battery is used as shown in Fig. 2.11. The specifications of this battery are listed in Table 2.3.



Fig. 2.11 12V battery ATLASBX ITX100

Table 2.3 Specifications of 12V battery ATLASBX ITX100

No.	Parameters	Values
1	Nominal Voltage (V)	12 V 100Ah
2	Weight	24.2 kg
3	Terminal type	Bolt terminal
4	Dimension (mm)	330 x 171 x 217

### 2.3 Basic terminologies of the 6LR

This section explains typical definitions and the concept of walking gait for the legged robot.

A *leg cycle* is composed of two phases as shown in Fig. 2.12.

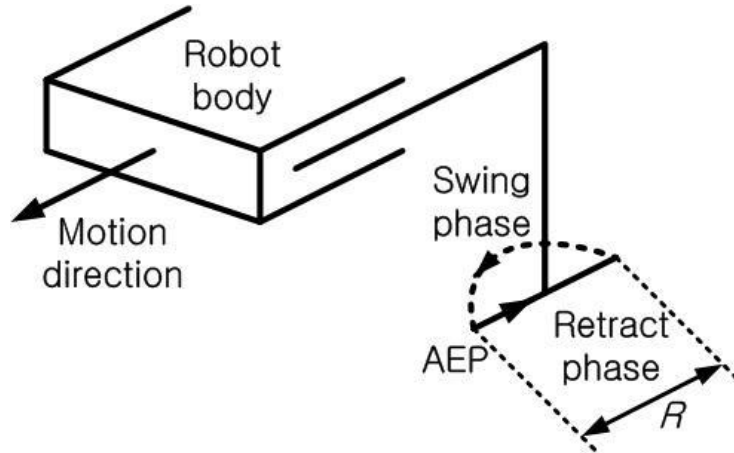


Fig. 2.12 Leg cycle of one leg

where  $R$  is the translational distance that the robot body moves after one cycle and called *stroke length*.

- The *swing phase* is the period while the leg moves from stand position to the *Anterior Extreme Position (AEP)* which is the position at the end of the swing phase.
- The *retract phase* is the period while the leg is in contact with the ground and propels the body.

The *cycle time*  $T$  is the sum of swing phase time and retract phase time.

$$T = T_{sw} + T_{rt} \quad (2.4)$$

where  $T_{sw}$  is the swing phase time and  $T_{rt}$  is the retract phase time.

The *duty factor*  $\rho = T_{rt} / T$  of a leg is the time duration of retract phase in a cycle time.

The *support polygon* is the polygon determined by the leg end effectors touching the ground. It is a dotted triangle in the tripod walking gait as shown in Fig. 2.13. There must be at least three touching points on the ground to support the 6LR.

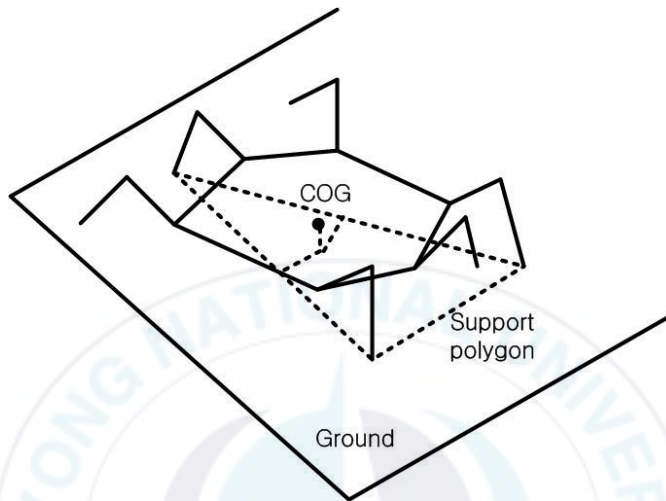


Fig. 2.13 Support polygon of the 6LR

For any support polygon, the distance between ‘the projection of the center of gravity (COG) on the support polygon’ and ‘the intersection of the front edge (in the walking direction) of the polygon with the longitudinal centerline of the body’ is called the *front stability margin*. The distance between ‘the projection of the center of gravity on the support polygon’ and ‘the intersection of the rear edge (in the opposite direction of walking) of the polygon with the longitudinal centerline of the body’ is called the *rear stability margin*. The definitions of the front and rear stability margins are shown in Fig. 2.14.

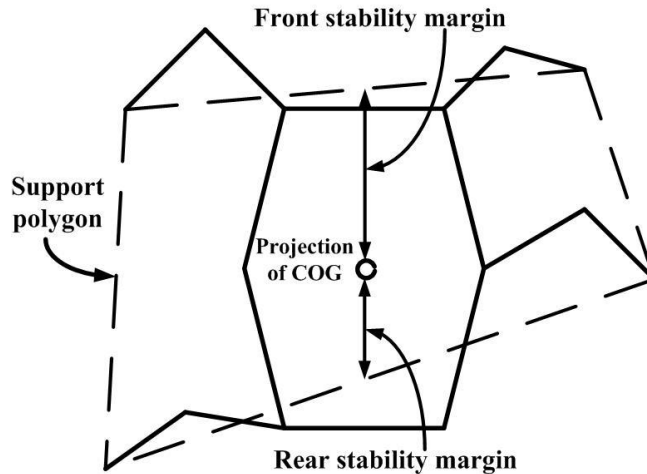


Fig. 2.14 Front and rear margins

*Longitudinal Stability Margin:* The minimum of the front and rear stability margins is called the longitudinal stability margin of the support polygon. (Longitudinal Gait) Stability Margin: The minimum of the longitudinal stability margins of all possible support polygons during walking according to a gait is called the stability margin of the gait. If the stability margin of a gait is larger than that of another gait, the former gait is called to be more stable than the latter.

**Statically Stable Gait:** A gait is said to be statically stable if its stability margin is greater than zero as in Fig. 2.14. Otherwise, the gait is said to be statically unstable as shown in Fig. 2.15. If a gait is stable, this means that the projection of center of gravity on the horizontal plane always remains inside the support polygon; otherwise, the center of gravity remains outside the support polygon in some instant times of the walk and the body falls down.

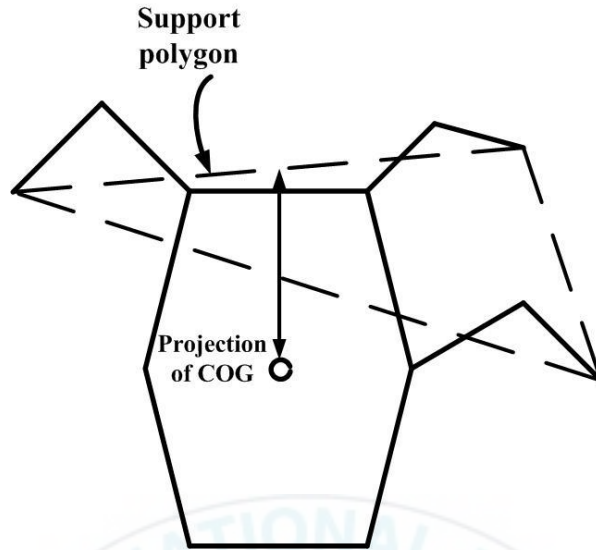


Fig. 2.15 Statically unstable gait

The attitude of the robot concerns the pitch and the roll of the robot with respect to the vertical global axis. The altitude of the robot is defined as the height of its center of mass with respect to the ground reference.

The posture of the robot is defined as the position of the six legs with respect to the main body.

The workspace of a leg is a reachable space by the end effector of the leg. This space has been restricted to a simple cylinder as shown in Fig. 2.16.

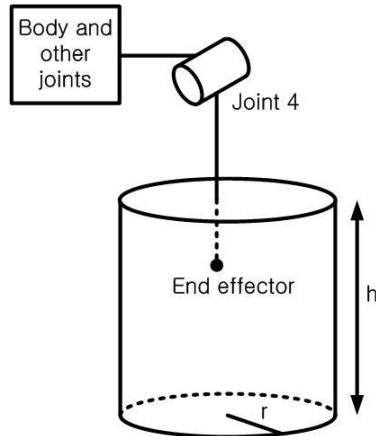


Fig. 2.16 Workspace of one leg

where  $r$  is the workspace radius and  $h$  is the workspace height.

In the swing phase, the end effector of each leg lifts up diagonally and moves to the AEP. In the retract phase, the end effector contacts the ground and moves back to the default standing position. The movement of the end effector in retract phase makes the body of the robot be propelled. The swing phase is designed as shown in Fig. 2.17. The swing phase is composed of two states: Diagonal lift up and Put down.

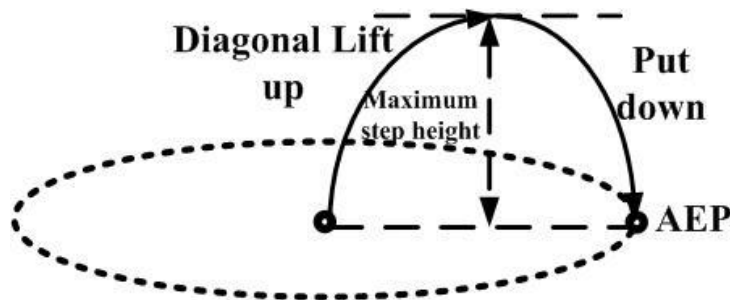


Fig. 2.17 Swing phase of step cycle of leg  $i$

A leg in the retract phase only moves when the other leg is in the swing phase as shown in Fig. 2.18.

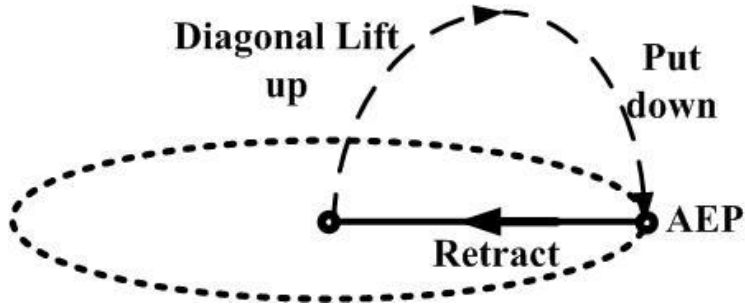


Fig. 2.18 Retract phase of step cycle of leg  $i$

## 2.4 Kinematic modeling of four joint legs

The six-legged robot consists of a trunk body and six legs. Each leg is constructed from four links and four rotation joints which are driven by DC servomotors. Fig. 2.19 shows the configuration of one leg of the developed six legged robot. The D-H convention is used to achieve kinematic modeling of each leg as follows:

- (1) Choose axis  $z_{ji}$  along the shaft of joint  $j$  of leg  $i$ .
- (2) Locate the origin  $O_{ji}$  at the intersection of axis  $z_{ji}$  with the common normal to axes  $z_{(j-1)i}$  and  $z_{ji}$ . Also, locate  $O'_{ji}$  at the intersection of the common normal line with axis  $z_{(j-1)i}$  from  $O_{ji}$ .
- (3) Choose axis  $x_{ji}$  along the common normal line to axes  $z_{(j-1)i}$  and  $z_{ji}$  with the direction from joint  $j$  to joint  $j+1$  of leg  $i$ .
- (4) Choose axis  $y_{ji}$  so as to complete a right-handed frame.
- (5)  $a_i$  is the distance between  $O_{ji}$  and  $O'_{ji}$ .
- (6)  $d_i$  is coordinate of  $O'_{ji}$  along  $z_{(j-1)i}$ ,

- (7)  $\alpha_{ji}$  is angle between  $z_{(i-1)i}$  and  $z_{ji}$  about axis  $x_{ji}$  to be taken positive when rotation is in counter-clockwise.
- (8)  $\theta_{ji}$  is angle between  $x_{(j-1)i}$  and  $x_{ji}$  about axis  $z_{(j-1)i}$  to be taken positive when rotation is in counter-clockwise.

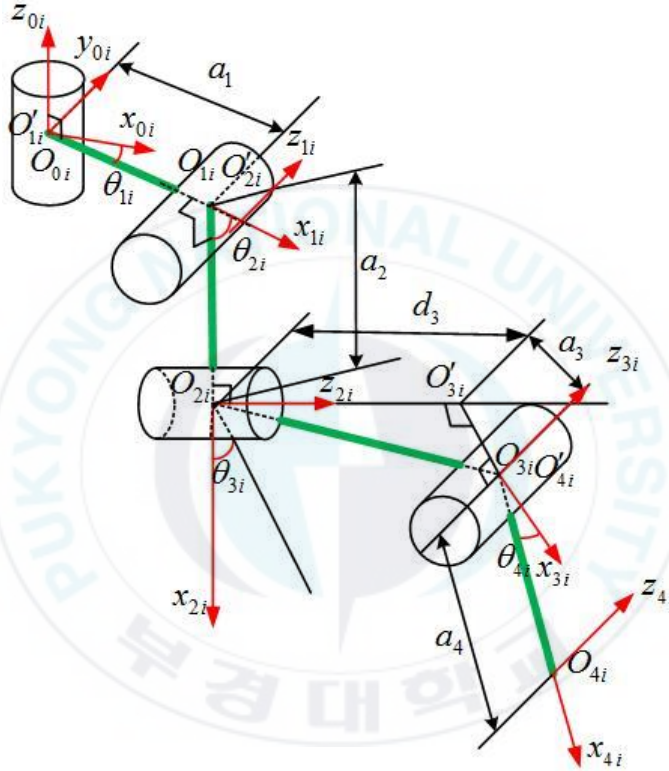


Fig. 2.19 Configuration of one leg

where

$O_{ji}$  : Origin of the joint  $j$  ( $j = 0, 1, 2, 3$ ) of leg  $i$  ( $i = 1, 2, 3, 4, 5, 6$ )

$\theta_{1i}$  : Rotational angle around  $z_{0i}$  axis of leg  $i$

$\theta_{2i}$  : Rotational angle around  $z_{1i}$  axis of leg  $i$

$\theta_{3i}$  : Rotational angle around  $z_{2i}$  axis of leg  $i$

$\theta_{4i}$  : Rotational angle around  $z_{3i}$  axis of leg  $i$

A coordinate of  $(x_{ji}y_{ji}z_{ji})$  is located on joint  $j$  of leg  $i$ . DH parameters are obtained by these coordinates for forward kinematic.

Table 2.4 D-H Parameters of 4-Link leg

Joint	$\theta_{ji}$	$\alpha_i$	$a_i$	$d_i$
0	$\theta_{1i}$	$-\pi/2$	$a_1$	0
1	$\theta_{2i}$	$\pi/2$	$a_2$	0
2	$\theta_{3i}$	$-\pi/2$	$a_3$	$d_3$
3	$\theta_{4i}$	0	$a_4$	0

The homogeneous transformation matrix can be obtained by D-H parameters as the following matrices.

$${}^0_1\mathbf{T}_i = \begin{bmatrix} c_{1i} & 0 & -s_{1i} & a_1c_{1i} \\ s_{1i} & 0 & c_{1i} & a_1s_{1i} \\ 0 & -1 & 0 & 0 \\ 0 & 0 & 0 & 1 \end{bmatrix} \quad (2.1)$$

$${}^1_2\mathbf{T}_i = \begin{bmatrix} c_{2i} & 0 & s_{2i} & a_2c_{2i} \\ s_{2i} & 0 & -c_{2i} & a_2s_{2i} \\ 0 & 1 & 0 & 0 \\ 0 & 0 & 0 & 1 \end{bmatrix} \quad (2.2)$$

$${}^2_3\mathbf{T}_i = \begin{bmatrix} c_{3i} & 0 & -s_{3i} & a_3c_{3i} \\ s_{3i} & 0 & c_{3i} & a_3s_{3i} \\ 0 & -1 & 0 & 0 \\ 0 & 0 & 0 & 1 \end{bmatrix} \quad (2.3)$$

$${}^3_4\mathbf{T}_i = \begin{bmatrix} c_{4i} & -s_{4i} & 0 & a_4c_{4i} \\ s_{4i} & c_{4i} & 0 & a_4s_{4i} \\ 0 & 0 & 1 & 0 \\ 0 & 0 & 0 & 1 \end{bmatrix} \quad (2.4)$$

where  $c_{ji} = \cos \theta_{ji}$ ,  $s_{ji} = \sin \theta_{ji}$  and  ${}^j_k \mathbf{T}_i$  is the transformation matrix from joint  $j$  coordinate system to joint  $k$  coordinate system of leg  $i$ .

The transformation matrix from joint 0 to end effector of leg  $i$  can be calculated as follows:

$${}^0_4 \mathbf{T}_i = {}^0_1 \mathbf{T}_i {}^1_2 \mathbf{T}_i {}^2_3 \mathbf{T}_i {}^3_4 \mathbf{T}_i \quad (2.5)$$

The end effector position vector with respect to joint 0 frame of leg  $i$   $\mathbf{p}_{ei}^0 = [x_{ei}^0 \ y_{ei}^0 \ z_{ei}^0]^T$  can be calculated by the first three elements of the last column of  ${}^0_4 \mathbf{T}_i$  also called forward kinematic equation  $k(\theta_i)$ . The forward kinematic equation is shown as follows:

$$k(\theta_i) = \mathbf{p}_{ei}^0 = [x_{ei}^0 \ y_{ei}^0 \ z_{ei}^0]^T \quad (2.6)$$

$$x_{ei}^0 = a_1 c_{1i} - a_4 c_{4i} (s_{1i} s_{3i} - c_{1i} c_{2i} c_{3i}) + a_2 c_{1i} c_{2i} + d_3 c_{1i} s_{2i} - a_3 s_{1i} s_{3i} + a_3 c_{1i} c_{2i} c_{3i} - a_4 c_{1i} s_{2i} s_{4i} \quad (2.7)$$

$$y_{ei}^0 = a_1 s_{1i} + a_4 c_{4i} (c_{1i} s_{3i} - s_{1i} c_{2i} c_{3i}) + a_2 s_{1i} c_{2i} + a_3 c_{1i} s_{3i} - d_3 s_{1i} s_{2i} + a_3 s_{1i} c_{2i} c_{3i} - a_4 s_{1i} s_{2i} s_{4i} \quad (2.8)$$

$$z_{ei}^0 = d_3 c_{2i} - a_2 s_{2i} - a_3 c_{3i} s_{2i} - a_4 c_{2i} s_{4i} - a_4 s_{2i} c_{3i} c_{4i} \quad (2.9)$$

where  $\boldsymbol{\theta}_i = [\theta_{1i}, \theta_{2i}, \theta_{3i}, \theta_{4i}]^T$  is angular position vector of each joint and is the solution of Eqs. (2.6) ~ (2.9) using the inverse kinematics

## 2.5 Kinematics of the six legged robot

The legs are attached to the platform of the robot. Such a solution implies the constant values in transformation of particular legs. The body frame assignment on the platform depends only on the geometrical dimensions of the robot as shown in Fig. 2.20 which  $W$  is the distance between Leg-L2 and Leg-R2,  $L$  is the length of the robot

and  $E$  is the distance between Leg-L1 and Leg-R1. It is assumed that the center of gravity is also the center of body of the 6LR.

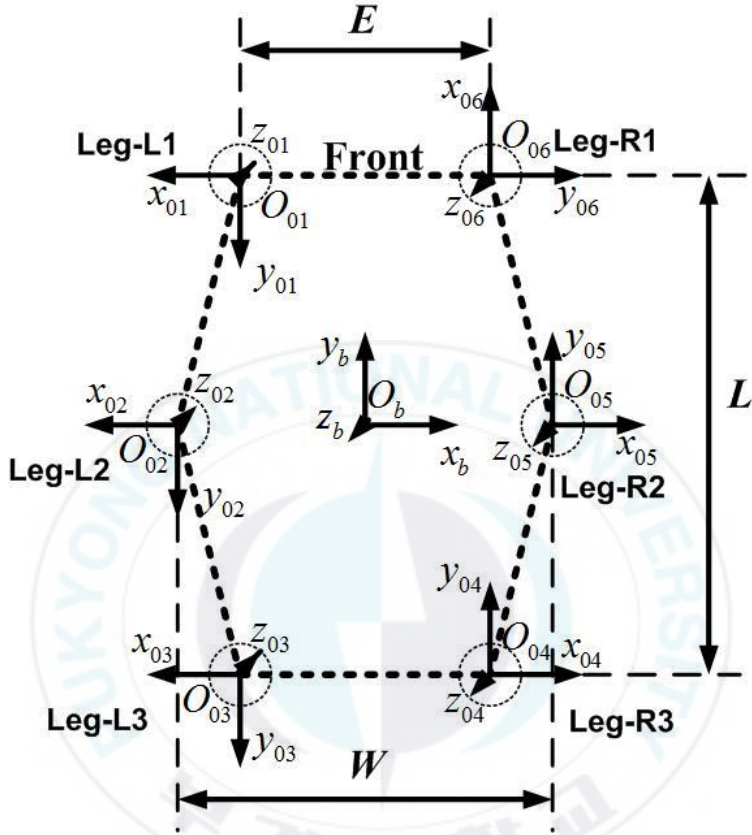


Fig. 2.20 Frame coordinates of the 6LR

where  $O_b, x_b, y_b, z_b$  is a body coordinate frame located on the center of body of the 6LR, and  $O_{ji}, x_{ji}, y_{ji}, z_{ji}$  is a leg coordinate frame located on joint  $j$  of leg  $i$ .

At swing phase, the shoulder of the leg is fixed and the end effector of the leg is moving. The end effector of the leg moves to the front. At the retract phase, the end effector moves to the rear. But in this phase, the leg is fixed to the ground so that the shoulder moves to

the front. The overall movement of the platform can be computed as a function of foot movement by using kinematics of the whole robot.

The homogeneous transformation matrices from body frame to the first joint of each leg can be derived as follows:

- The body frame transformation matrix to Leg-L1 frame by translating a distance ( $E/2$ ) along  $x_b$  axis and a distance ( $L/2$ ) along  $y_b$  axis is expressed by

$${}^b_0\mathbf{T}_1 = \begin{bmatrix} 1 & 0 & 0 & E/2 \\ 0 & 1 & 0 & L/2 \\ 0 & 0 & 1 & 0 \\ 0 & 0 & 0 & 1 \end{bmatrix} \quad (2.10)$$

- The body frame transformation matrix to Leg-L2 frame by translating a distance ( $W/2$ ) along  $x_b$  axis is expressed by

$${}^b_0\mathbf{T}_2 = \begin{bmatrix} 1 & 0 & 0 & W/2 \\ 0 & 1 & 0 & 0 \\ 0 & 0 & 1 & 0 \\ 0 & 0 & 0 & 1 \end{bmatrix} \quad (2.11)$$

- The body frame transformation matrix to Leg-L3 frame by translating a distance ( $E/2$ ) along  $x_b$  axis and a distance ( $L/2$ ) along inverse direction of  $y_b$  axis is expressed by

$${}^b_0\mathbf{T}_3 = \begin{bmatrix} 1 & 0 & 0 & E/2 \\ 0 & 1 & 0 & -L/2 \\ 0 & 0 & 1 & 0 \\ 0 & 0 & 0 & 1 \end{bmatrix} \quad (2.12)$$

- The body frame transformation matrix to Leg-R3 frame by translating a distance ( $E/2$ ) along inverse direction of  $x_b$  axis

and a distance  $(L/2)$  along inverse direction of  $y_b$  axis and rotating an angle  $\pi$  about  $z_b$  axis is expressed by

$${}^b_0\mathbf{T}_4 = \begin{bmatrix} -1 & 0 & 0 & -E/2 \\ 0 & -1 & 0 & -L/2 \\ 0 & 0 & 1 & 0 \\ 0 & 0 & 0 & 1 \end{bmatrix} \quad (2.13)$$

- The body frame transformation matrix to Leg-R2 frame by translating a distance  $(W/2)$  along inverse direction of  $x_b$  axis and rotating an angle  $\pi$  about  $z_b$  axis is expressed by

$${}^b_0\mathbf{T}_5 = \begin{bmatrix} -1 & 0 & 0 & -W/2 \\ 0 & -1 & 0 & 0 \\ 0 & 0 & 1 & 0 \\ 0 & 0 & 0 & 1 \end{bmatrix} \quad (2.14)$$

- The body frame transformation matrix to Leg-R1 frame by translating a distance  $(E/2)$  along inverse direction of  $x_b$  axis and a distance  $(L/2)$  along  $y_b$  axis and rotating an angle  $\pi$  about  $z_b$  axis is expressed by

$${}^b_0\mathbf{T}_6 = \begin{bmatrix} -1 & 0 & 0 & -E/2 \\ 0 & -1 & 0 & L/2 \\ 0 & 0 & 1 & 0 \\ 0 & 0 & 0 & 1 \end{bmatrix} \quad (2.15)$$

The end effector position vector of each leg with respect to body frame can be derived from transformation matrix as follows:

$$\tilde{\mathbf{p}}_{ei}^b = {}^b_0\mathbf{T}_i \tilde{\mathbf{p}}_{ei}^0 \quad (2.16)$$

where  $\tilde{\mathbf{p}}_{ei}^b = \begin{bmatrix} \mathbf{p}_{ei}^b \\ 1 \end{bmatrix}$ ,  $\tilde{\mathbf{p}}_{ei}^0 = \begin{bmatrix} \mathbf{p}_{ei}^0 \\ 1 \end{bmatrix}$ , and  $\mathbf{p}_{ei}^b$  is the position vector of the end effector with respect to body frame of leg  $i$ .

From Eq. (2.16), the end effector position vector of leg  $i$  with respect to joint 0 can be expressed as follows:

$$\tilde{\mathbf{p}}_{ei}^0 = {}^b\mathbf{T}_i^T \tilde{\mathbf{p}}_{ei}^b \quad (2.17)$$



## Chapter 3: CPG Model and Parameters Analysis

This chapter describes CPG model used in this thesis to generate stable rhythmic signals. One CPG model is composed of two identical neurons. Also the parameters of the CPG model are analyzed in order to generate stable rhythmic reference signals.

### 3.1 CPG model

The neural oscillator model proposed by Matsuoka is the best known CPG model in robotics engineering applications. It is composed of two identical neurons. The neuron model mimics the average of spike activity of the biological neuron. The dynamics of the two neurons are given by the following differential equations [31].

$$\begin{aligned} T_r \dot{x}_i(t) &= -x_i - w_{ij} y_j(t) - \beta v_i(t) + s_0 \\ T_a \dot{v}_i(t) &= -v_i(t) + y_i(t) \\ y_i(t) &= g(x_i(t)), \quad g(x_i(t)) \triangleq \max(x_i(t), 0) \end{aligned} \tag{3.1}$$

where  $x_i$  is the inner state of the  $i^{\text{th}}$  neuron;  $v_i$  is a variable which represents the degree of the adaptation or self-inhibition effect of the  $i^{\text{th}}$  neuron;  $T_r$  and  $T_a$  are time constants of  $x_i$  and  $v_i$ ;  $w_{ij}$  is the connection weight between neurons of the  $i^{\text{th}}$  and  $j^{\text{th}}$  neuron oscillator;  $\beta$  is a constant representing the degree of the self-inhibition influence on the inner state; and  $s_0$  is an external input with a constant rate;  $y_i$  is the output of the neuron.

Because it simulates neuron's properties more precisely, Matsuoka's model has been widely applied to locomotion control of

legged robots. Based on Matsuoka's model, Taga et al. proposed a similar model, which used a set of inhibitory connected neuron oscillators to build a network. Kimura et al. constructed a neural system based on the neural oscillator proposed by Matsuoka and Taga. This CPG model consists of two mutually inhibiting neurons as shown in Fig 3.1. In Kimura's model, the linear summation of the outputs of the two neurons is used as system's output. Each neuron is represented by the following nonlinear differential equations:

$$\begin{cases} \tau \dot{u}_{\{e,f\}i} = -u_{\{e,f\}i} - w_{fe} y_{\{f,e\}i} - \beta v_{\{e,f\}i} + \sum_{j=1}^n w_{ij} y_{\{e,f\}j} + u_0 + feed_{\{e,f\}i} \\ \tau' \dot{v}_{\{e,f\}i} = -v_{\{e,f\}i} + y_{\{e,f\}i} \\ y_{\{e,f\}i} = \max(u_{\{e,f\}i}, 0) \\ (i, j = 1, \dots, n) \\ y_i = y_{fi} - y_{ei} \end{cases} \quad (3.2)$$

Where the subscripts  $e$ ,  $f$ ,  $i$  and  $j$  denote an extensor neuron, the  $i^{\text{th}}$  neuron oscillator and  $j^{\text{th}}$  neuron oscillator, respectively.  $u_{\{e,f\}i}$  is  $u_{ei}$  or  $u_{fi}$ , that is the inner state of an extensor neuron or a flexor neuron of the  $i^{\text{th}}$  neuron oscillator;  $v_{\{e,f\}i}$  is a variable representing the degree of the self-inhibition effect of the neuron;  $y_{\{e,f\}i}$  is  $y_{ei}$  or  $y_{fi}$ , and  $y_{\{f,e\}i}$  is  $y_{fi}$  or  $y_{ei}$ , that are the outputs of extensor or flexor neurons;  $u_0$  is an external input with a constant rate;  $feed_{\{e,f\}i}$  is a feedback signal from the robot that is a joint angle, angular velocity and so on; and  $\beta$  is a constant representing the degree of the self-inhibition influence on the inner state. The quantities  $\tau$  and  $\tau'$  are time constant of  $u_{\{e,f\}i}$  and  $v_{\{e,f\}i}$ ;  $w_{fe}$  is a connection weight between flexor and extensor neurons;  $w_{ij}$  is a connection weight between

neurons of  $i^{th}$  and  $j^{th}$  neuron oscillator.  $y_i$  is the output of a CPG model.

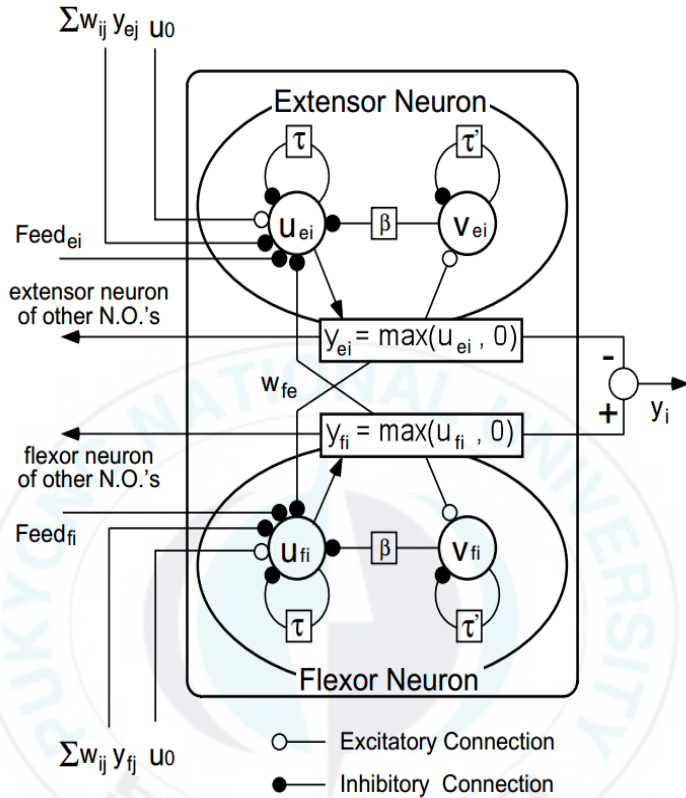


Fig. 3.1 Neural oscillator as a model of CPG

Neuronal oscillator models have clear biological meanings, especially Matsuoka's model. This model can easily couple the feedback information of environment and the higher level orders. In Matsuoka's model, sensory feedbacks can be integrated to the CPG network through the term  $feed_{\{e,f\}i}$  and the external input term  $u_0$  from the higher level control nervous system. This provides the opportunity to obtain mutual entrainment between the CPG network and the mechanical body.

### 3.2 Parameters analysis

Since several parameters are involved in Matsuoka models, selecting proper parameter is essential to the CPG inspired control method. Also the performance analysis of the oscillators becomes the major difficulty for engineering application. We must grasp the relationships of the parameters and the important qualities such as frequency, amplitude, phase relationships between the neurons and the waveform of the output signals. The dynamics of the model is complicated and it is difficult to use the systematic method to do further researches. K. Matsuoka linearized the equation and deduced some conditions of the equation producing stable oscillations [31]. M. M. Williamson and J. H. Jianjuen adopted the describing function method to analyze the equation, to predict stability and steady state motion and to complete parameter regulation of rhythmic motion control system [32-33]. A. M. Arsenio combined multi-input describing functions method with conventional Fourier transform and stability criterions to establish algebraic method for system dynamics analysis and parameter regulation [34]. H. Yuasa and M. Ito used the phase plane and potential function in the relative phase space to describe dynamics of CPG network. They proposed an approach to design pattern generator [35]. In engineer practices, the trial-and-error method and the genetic algorithm are often adopted to realize parameter setting of CPG equation [36-38]. However, these methods are too complicated and difficult to comprehensively describe dynamics of the CPG equation and effect trends of each parameter, which results are difficult for the study of CPG nerve circuit and engineering applications of the biological control mechanism.

In this chapter, a method to do numerical simulation to identify effect trends of parameters through computer is described. Because of the complicated coupling relation between parameters of CPG equation, this thesis mainly adopts the single-parameter-analysis method which is fixing other parameters and studying the influence on amplitude, period, phase and waveform of the output by changing one parameter. Default values of the parameters in (3.2) are  $\tau = 0.04$ ;  $\tau' = 0.6$ ;  $\beta = 5$ ;  $u_0 = 2$ ;  $w_{fe} = 2$ . There are no feedbacks in the simulation, so the value of  $feed_{\{e,f\}i}$  is 0.

### 3.2.1 Parameter $u_0$

The parameter  $u_0$  is a constant input corresponding to command signal from higher nerve center. The value of  $u_0$  is set to  $-1, 0, 1, 2, 4$ . Fig. 3.2 shows outputs of CPG according to  $u_0$  value. From Fig. 3.2, the value of  $u_0$  has no relation with the oscillation period. Also,  $u_0$  is a relatively independent parameter and mainly determines the output amplitude. When  $u_0 \leq 0$ , the outputs go to 0 rapidly. In order to yield a stable oscillation, the span of  $u_0$  should be set to  $(0, +\infty)$ .

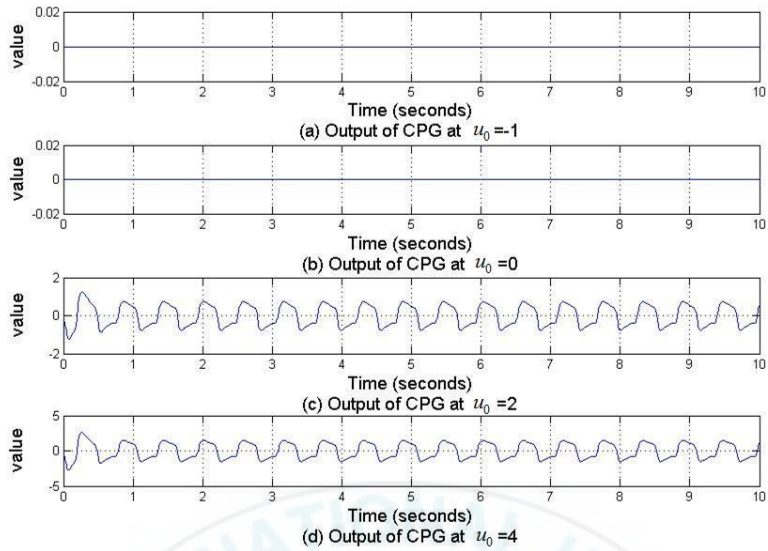


Fig. 3.2 Output of CPG according to  $u_0$  value

### 3.2.2 Parameter $\beta$

Fig. 3.3 shows output of CPG according to  $\beta$  value. From Fig. 3.3, when  $\beta$  becomes larger, the period and the amplitude become smaller rapidly. The parameter  $\beta$  is the adaptive coefficient and inhibits output increases of neuron, so the larger  $\beta$  is, the smaller the output amplitude and the period of oscillator is.

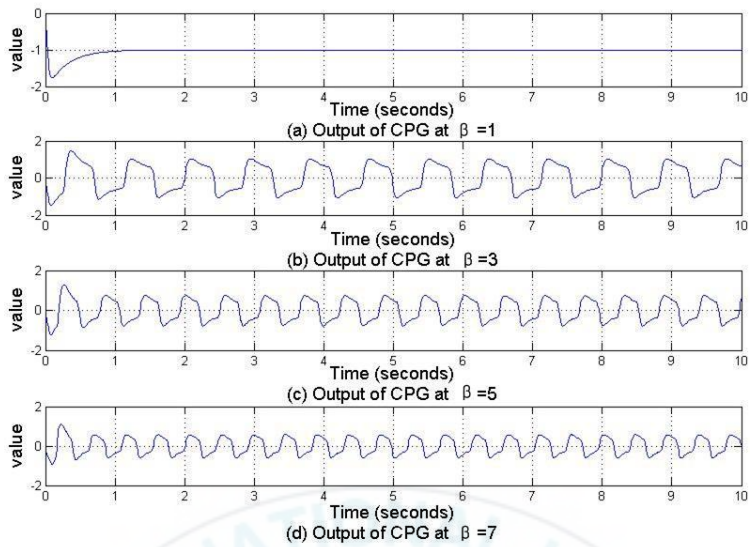


Fig. 3.3 Output of CPG according to  $\beta$  value

### 3.2.3 Parameter $w_{fe}$

Fig. 3.4 shows output of CPG according to  $w_{fe}$  value. From Fig. 3.4, when  $w_{fe}$  becomes larger, the period and the amplitude become larger rapidly. And the slope coefficient gradually becomes smaller as the value of  $w_{fe}$  become larger.

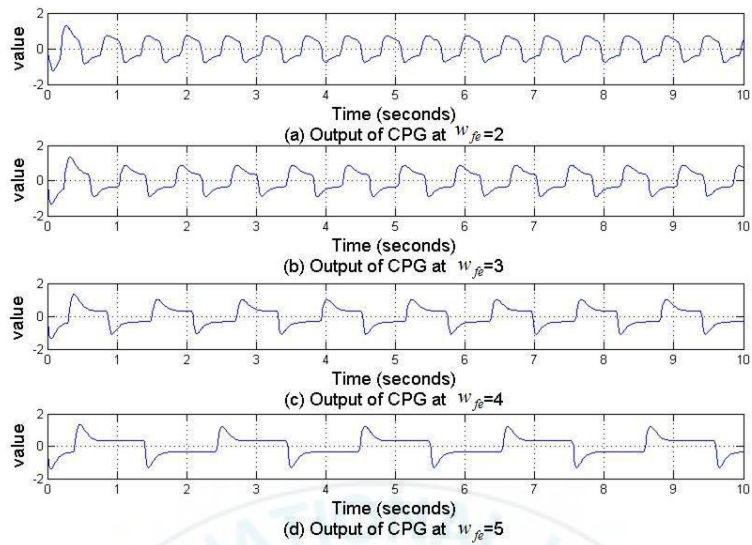


Fig. 3.4 Output of CPG according to  $w_{fe}$  value

### 3.2.4 Parameter $\tau$

Fig. 3.4 shows output of CPG according to  $\tau$  value. From Fig. 3.5, parameter  $\tau$  is related to the period of CPG output. When other parameters are set to default values, the adjustable extent of  $\tau$  should be set bigger than 0. When  $\tau$  becomes larger, the period of CPG output becomes larger.

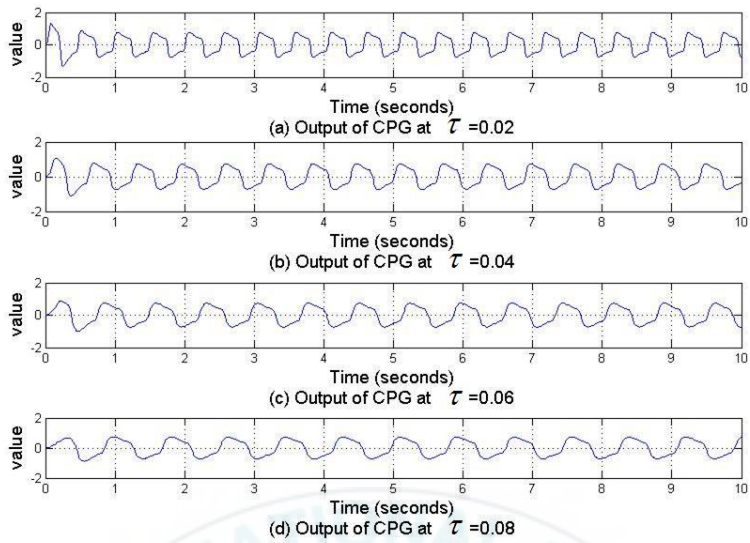


Fig. 3.5 Output of CPG according to  $\tau$  value

### 3.2.5 Parameter $\tau'$

Fig. 3.6 shows output of CPG according to  $\tau'$  value. From Fig. 3.6, parameter  $\tau'$  is also related to the period of CPG output. When other parameters are set to default values, the adjustable extent of  $\tau'$  should be set bigger than 0. When  $\tau'$  becomes larger, the period of CPG output becomes larger.

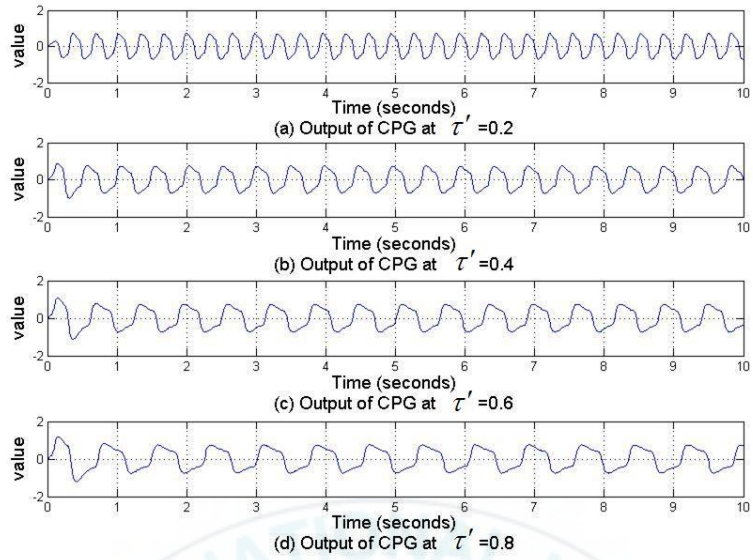


Fig. 3.6 Output of CPG according to  $\tau'$  value

# Chapter 4: Gait Planning Based on CPG Network and Controller Design

This chapter introduces a CPG network which is used for gait planning of six CPG models. Different outputs of CPG network correspond to different gaits. In this chapter, three kinds of gaits for a six-legged robot are designed by changing the connecting weight of CPG network such as wave gait, quadruped gait and tripod gait. The output signals of CPG network are redesigned for a workspace trajectory of each leg's end effector by using a mapping function.

## 4.1 CPG network

The CPG network is constructed by using six inhibitory connecting CPG models. One CPG model is used to control one leg. Using six Matsuoka oscillators, a holosymmetric CPG network for a hexapod robot is built. A 6\*6 matrix is used as the connecting weight of CPG network as shown in Fig. (4.1).  $w_{ij}$  is defined as the connecting weight from oscillator  $j$  to  $i$ . Three principles to set  $w_{ij}$  are proposed as follows:

- (a) There is no self-inhibition in CPG network. So self-connecting weight of each leg is 0. All elements in the leading diagonal of  $w_{ij}$  are 0.
- (b) Inhibition between any two legs is reciprocal and coequal. So  $w_{ij}$  is a symmetric matrix.

(c) If two legs are in same phase, exciting connections are adopted between the two oscillators and their corresponding elements are set to 1. If two legs are in different phase, inhibiting connections are adopted and their corresponding elements are set to -1.

Fig. 4.1 shows the CPG network of the six-legged walking robot. In Fig. 4.1, E.N is extensor neural, and F.N is flexor neural. The connecting weight matrix based on these principles can describe the phase relationship between oscillators, and has direct relationship with the gait of the hexapod robot.

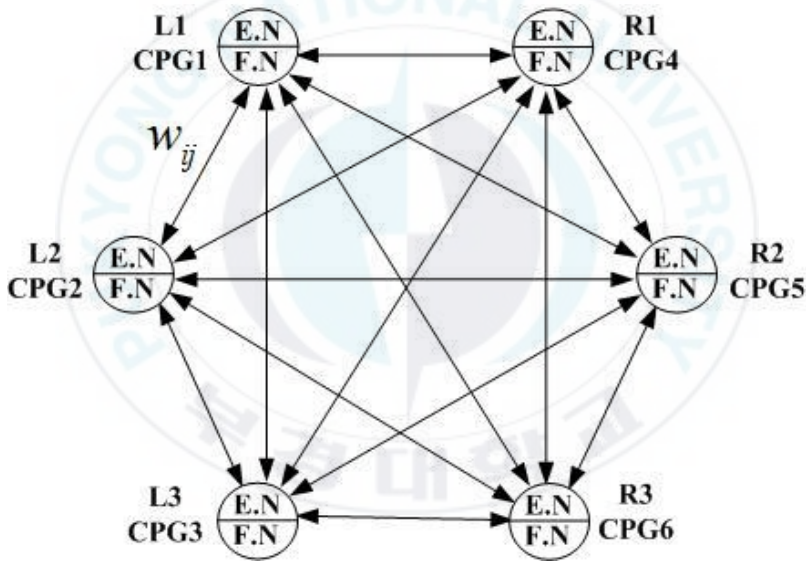


Fig. 4.1 CPG network of the six-legged walking robot

#### 4.1.1 Wave gait

When a robot walks at wave gait, the moving leg's sequence in Fig. 4.2 can be described as follows: At first, Leg-L1 is at swing phase, Leg-L2, Leg-L3 , Leg-R1, Leg-R2 and Leg-R3 are at retract

phase. After  $1/6$  cycle, Leg-R1 are at swing phase, and Leg-L1, Leg-L2, Leg-L3, Leg-R2, Leg-R3 are at retract phase. After  $1/6$  cycle, Leg-L3 are at swing phase, and Leg-L1, Leg-L2, Leg-R1, Leg-R2, Leg-R3 are at retract phase. After  $1/6$  cycle, Leg-L2 are at swing phase, and Leg-L1, Leg-L3, Leg-R1, Leg-R2, Leg-R3 are at retract phase. After  $1/6$  cycle, Leg-R2 are at swing phase, and Leg-L1, Leg-L2, Leg-L3, Leg-R1, Leg-R3 are at retract phase. After  $1/6$  cycle, Leg-R3 are at swing phase, and Leg-L1, Leg-L2, Leg-L3, Leg-R1, Leg-R2 are at retract phase. The sequence is repeated every cycle.

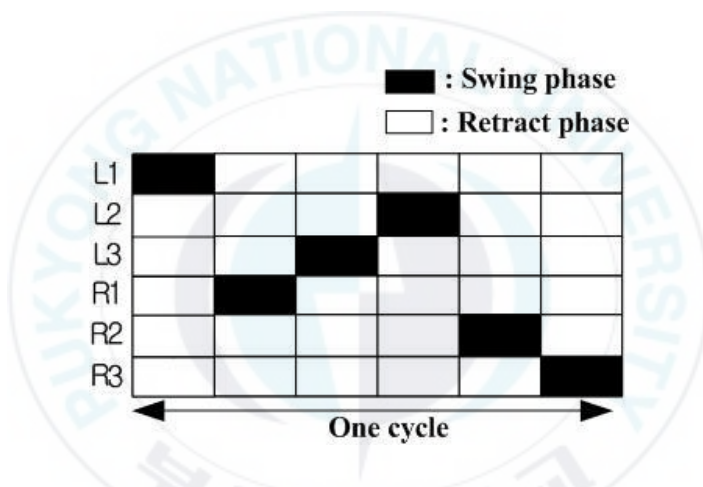


Fig. 4.2 Walking cycle of the wave gait

Each state time in one step cycle  $T$  of the wave gait is designed as shown in Fig. 4.3.

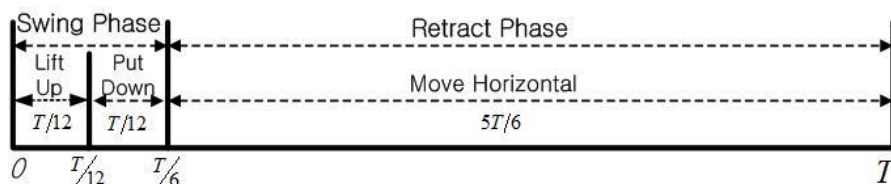


Fig. 4.3 Each state time in one cycle time of the wave gait

The topology of CPG network for wave gait is shown as Fig. 4.4. In Fig. 4.4, all CPG models are connected by inhibitory connection.

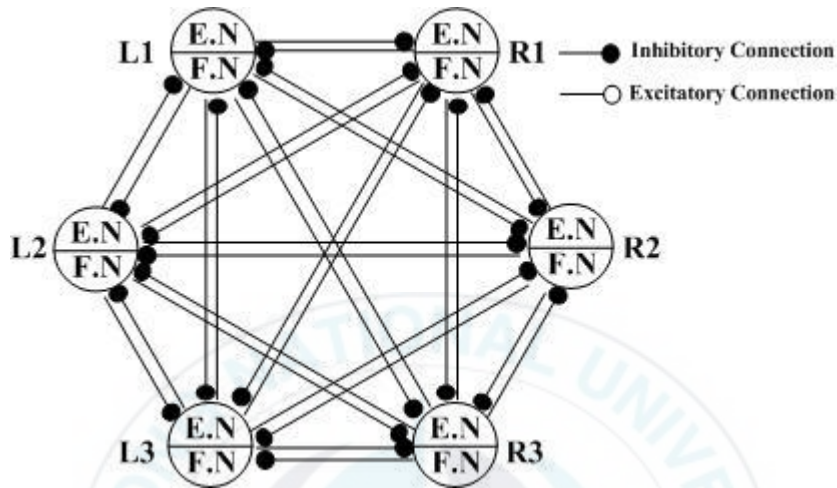


Fig. 4.4 Topology of CPG network for the wave gait

#### 4.1.2 Quadruped gait

When robot walks at quadruped gait, the moving leg's sequence in Fig. 4.5 can be described as follows: At first, Leg-L1 and Leg-R2 are at swing phase, Leg-L2, Leg-L3, Leg-R1 and Leg-R3 are at retract phase. After 1/3 cycle, Leg-R1 and Leg-R2 are at swing phase, and Leg-L1, Leg-L3, Leg-R2, Leg-R3 are at retract phase. After 1/3 cycle, Leg-L3 and Leg-R1 are at swing phase, and Leg-L1, Leg-L2, Leg-R2, Leg-R3 are at retract phase. The sequence is repeated every cycle.

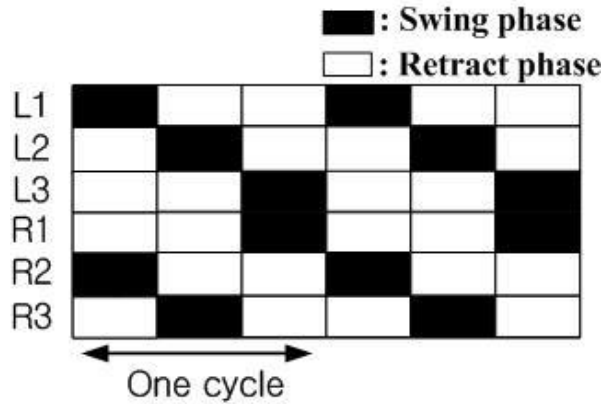


Fig. 4.5 Walking cycle of the quadruped gait

Each state time in one step cycle  $T$  of the quadruped gait is designed as shown in Fig. 4.6.



Fig. 4.6 Each state time in one cycle time of the quadruped gait

The topology of CPG network for quadruped gait is shown as Fig 4.7. In Fig. 4.7, L1 and R2, L2 and R3, and L3 and R1 are connected by excitatory connection, respectively.

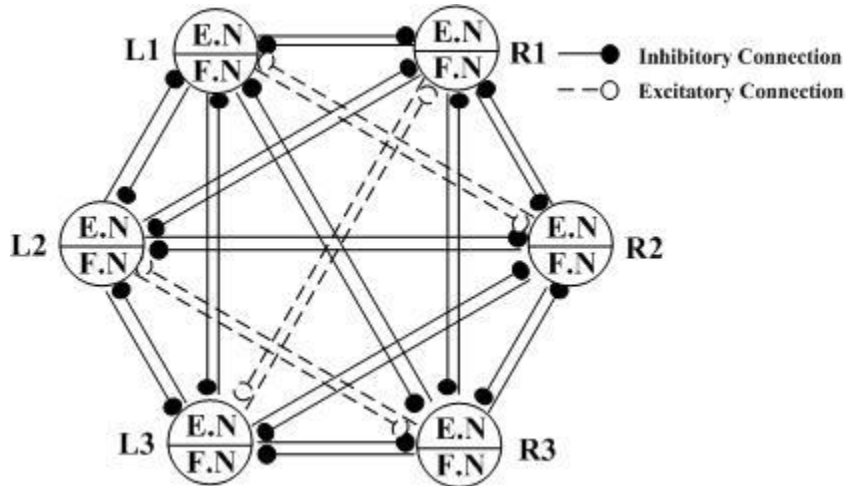


Fig. 4.7 Topology of CPG network for the quadruped gait

### 4.1.3 Tripod gait

Among all these gaits, tripod gait is chosen as the walking gait for 6LR in this thesis. The walking cycle imitating this gait is shown in Fig. 4.8. When the robot walks, three legs support the body and the other three legs lift up and move for next walking motion. The moving leg's sequence in Fig. 4.8 can be described as follows: At first, Leg-L1, Leg -L3 and Leg-R2 are at swing phase, and Leg-L2, Leg-R1 and Leg-R3 are at retract phase. After a half of cycle, Leg-L1, Leg -L3 and Leg-R2 are at retract phase, and Leg-L2, Leg-R1 and Leg-R3 are at swing phase. The sequence is repeated every cycle.

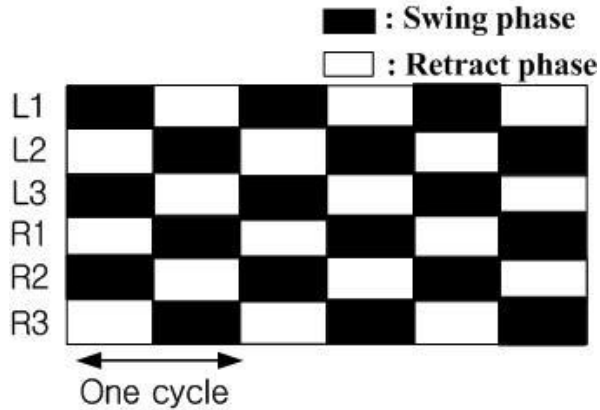


Fig. 4.8 Walking cycle of the tripod gait

Each state time in one step cycle  $T$  of the tripod gait is designed as shown in Fig. 4.9.

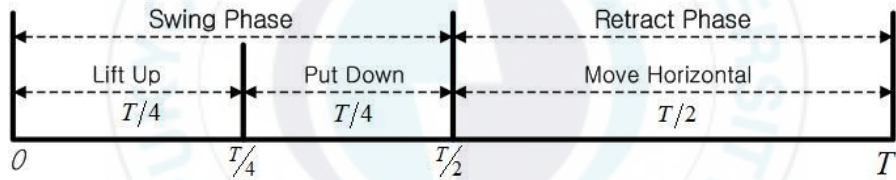


Fig. 4.9 Each state time in one cycle time of the tripod gait

The topology of CPG network for tripod gait is shown as Fig. 4.10. In Fig. 4.10, L1, R2 and L3, and L2, R1 and R3 are connected by excitatory connection, respectively.

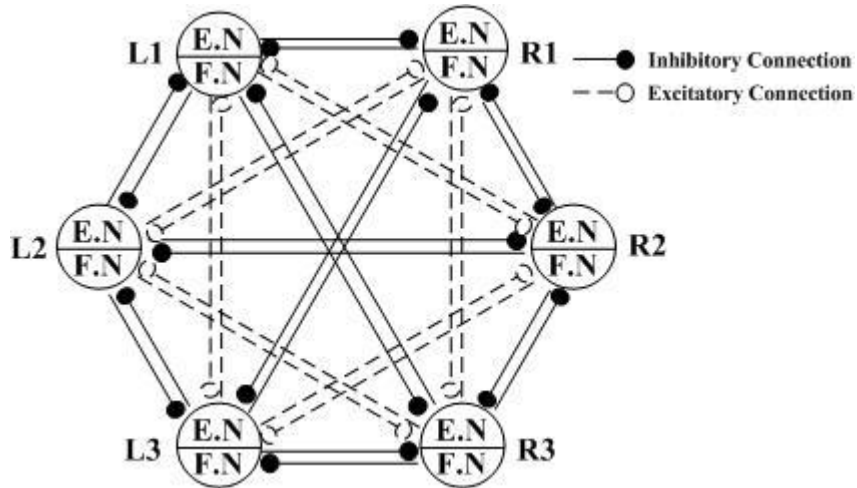


Fig. 4.10 Topology of CPG network for the tripod gait

## 4.2 Mapping function

In this section, instead of directly controlling the joint angle using the output of CPG network, a mapping function is designed to map the signal of CPG network into workspace trajectories of the corresponding legs. The end effector trajectories are functions of the output signals of the corresponding CPG oscillators. In addition, the mapping function offers an adaptive control system to the six legged robot since the workspace trajectories can be adapted by the parameters of CPG model. Because the output of CPG network is not steady at the beginning, so the mapping process begins from the steady states of the CPG network output.

The workspace trajectory for the end effector of each leg is designed as a set of desired position vector  $P_{di}^b(t)$  at time  $t$  for the

end effector to track. Fig. 4.11 shows the end effector trajectory of one leg of the 6LR.

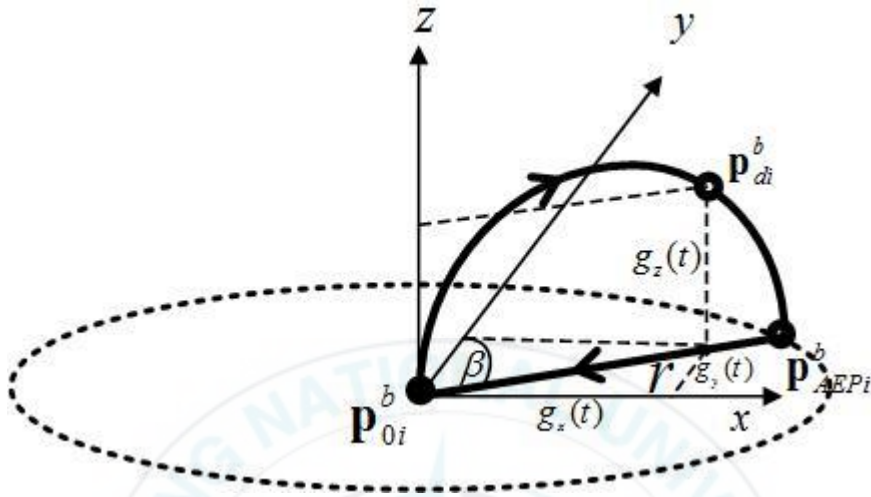


Fig. 4.11 End effector trajectory of one leg of the 6LR

where  $(x, y, z)$  is the coordinate of the end effector.  $(g_x, g_y, g_z)$  is the position coordinate of the end effector.  $\beta$  is the orientation angle of 6LR.  $r$  is the distance of one step.  $P_{0i}^b$  is the default standing position vector of leg  $i$  with respect to body frame.  $P_{AEPi}^b$  is the Anterior Extreme Position vector of leg  $i$ .

For each leg, to achieve AEP from the default standing position, the AEP vector of leg  $i$ ,  $P_{di}^b$  is calculated as follows:

$$P_{di}^b(t) = P_{0i}^b + T_m(t), T_m = \begin{bmatrix} g_x(t) \\ g_y(t) \\ g_z(t) \end{bmatrix} \quad (4.1)$$

where

$T_m$  : Translational movement vector with orientation angle  $\beta$  and step distance  $r$

$g_x$  : Translational movement of the end effector in  $x$  direction

$g_y$  : Translational movement of the end effector in  $y$  direction

$g_z$  : Translational movement of the end effector in  $z$  direction

The path of the end effector of each leg is designed as follows:

The mapping functions of the end effector for tripod gait are shown as Eq. (4.2).

$$\begin{cases} g_x(t) = r \sin \beta(t/T_{sw}) \\ g_y(t) = r \cos \beta(t/T_{sw}) \\ g_z(t) = k_z y(t) \\ 0 \leq t \leq T_{sw} \end{cases} \quad (4.2)$$

$$\text{where } \begin{cases} \text{wave gait:} & T_{sw} = (1/6)T \\ \text{quadruped gait:} & T_{sw} = (1/3)T \\ \text{tripod gait:} & T_{sw} = (1/2)T \end{cases}$$

The mapping functions of end effector are shown as Eq. (4.3).

$$\begin{cases} g_x(t) = r \sin \beta[(T-t)/T_r] \\ g_y(t) = r \cos \beta[(T-t)/T_r] \\ g_z(t) = 0 \\ T_{sw} \leq t \leq T \end{cases} \quad (4.3)$$

$$\text{where } \begin{cases} \text{wave gait:} & T_r = (5/6)T \\ \text{quadruped gait:} & T_r = (2/3)T \\ \text{tripod gait:} & T_{sw} = (1/2)T \end{cases}$$

$y(t)$  is the output of CPG network,  $k_z$  is the amplitude gain coefficients,  $t$  is the time that corresponds to the pointer of the mapping process.  $T_{sw}$  is the time of the swing phase for duration of  $y(t) > 0$ .  $T_r$  is the time of the retract phase for the duration of  $y(t) \leq 0$ .

In this thesis, the orientation angle  $\beta = 0(\text{rad})$ . Using the mapping function, the signal of the CPG network output rather than 0 ( $y(t) > 0$ ) is mapped to the swing phase, and the signal of the CPG network output less or equal to 0 ( $y(t) \leq 0$ ) is mapped to the retract phase.

### 4.3 Workspace trajectory tracking controller design

This section introduces a trajectory tracking controller for six legs to follow the trajectory designed by CPG network and mapping function. By using the designed mapping function, the workspace trajectory of the end effector is obtained. Therefore, forward kinematics and inverse kinematics equations are used for calculating the angle of each joint corresponding to a given end effector position.

However, it is difficult and complex to get the angle of four rotational joints by using inverse kinematics because of the equations of the inverse kinematics are nonlinear, and it is not always possible to find their solution. Also there may exist multiple solutions. To solve this problem, the differential kinematics algorithm is used to solve inverse kinematics problem easily.

For one leg of the 6LR, the end effector position error vector between the desired end effector position vector and the end effector position vector of leg  $i$  with respect to body frame is defined as follows:

$$\mathbf{e}_i^b = \mathbf{p}_{di}^b - \mathbf{p}_{ei}^b \quad (4.4)$$

where  $\mathbf{p}_{di}^b = [x_{di}^b \ y_{di}^b \ z_{di}^b]^T$  is the desired end effector position vector with respect to body frame of leg  $i$  as shown in Fig. 4.12.

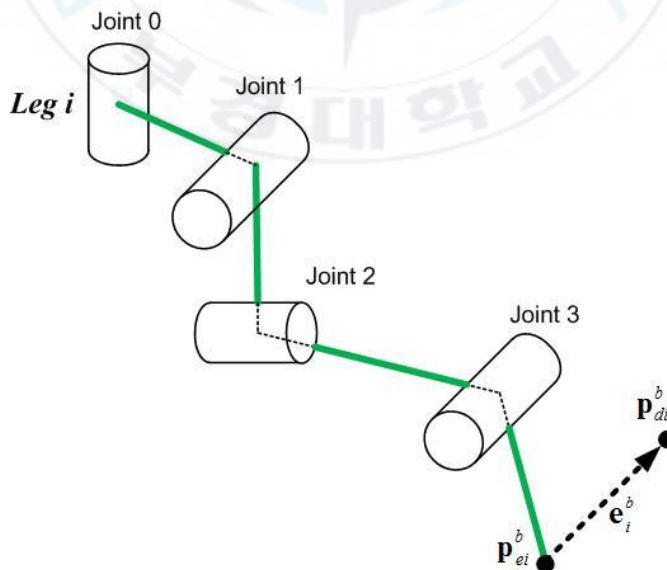


Fig. 4.12 End effector position control of leg  $i$

In this thesis, to keep the end effector in the desired position, we only consider the Jacobian relating the translational velocity of the end effector with the joint angular velocity. The translational velocity of the end effector can be expressed as the time derivative of the end effector position vector of leg  $i$  with respect to body frame  $\mathbf{p}_{ei}^b$ .

$$\dot{\mathbf{p}}_{ei}^b = \frac{\partial \mathbf{p}_{ei}^b}{\partial \boldsymbol{\theta}_i} \dot{\boldsymbol{\theta}}_i = \mathbf{J}_{Ai}^b(\boldsymbol{\theta}_i) \dot{\boldsymbol{\theta}}_i \quad (4.5)$$

where  $\mathbf{J}_{Ai}^b(\boldsymbol{\theta}_i)$  is the analytical Jacobian of  $\mathbf{p}_{ei}^b$  with respect to  $\theta_i$  as:

$$\mathbf{J}_{Ai}^b(\boldsymbol{\theta}_i) = \frac{\partial \mathbf{p}_{ei}^b}{\partial \boldsymbol{\theta}_i} = \frac{\partial k(\boldsymbol{\theta}_i)}{\partial \boldsymbol{\theta}_i} \quad (4.6)$$

The time derivative of Eq. (4.4) is written as

$$\dot{\mathbf{e}}_i^b = \dot{\mathbf{p}}_{di}^b - \dot{\mathbf{p}}_{ei}^b \quad (4.7)$$

From Eq. (4.5), Eq. (4.7) can be written as follows:

$$\dot{\mathbf{e}}_i^b = \dot{\mathbf{p}}_{di}^b - \mathbf{J}_{Ai}^b(\boldsymbol{\theta}_i) \dot{\boldsymbol{\theta}}_i \quad (4.8)$$

The candidate Lyapunov function (clf) can be chosen in the following positive definite quadratic form:

$$V_i(\mathbf{e}_i^b) = \frac{1}{2} (\mathbf{e}_i^b)^T \mathbf{K} \mathbf{e}_i^b \quad (4.9)$$

where  $\mathbf{K}$  is a symmetric positive definite matrix.

This function is so that:

$$V_i(\mathbf{e}_i^b) > 0 \text{ for } \forall \mathbf{e}_i^b \neq 0, V_i(0) = 0 \quad (4.10)$$

Differentiating Eq. (4.9) with respect to time and substituting Eq. (4.8) into it, the derivative of the clf can be derived as follows:

$$\dot{V}_i(\mathbf{e}_i^b) = (\mathbf{e}_i^b)^T \mathbf{K} \dot{\mathbf{e}}_i^b = (\mathbf{e}_i^b)^T \mathbf{K} \dot{\mathbf{p}}_{di}^b - (\mathbf{e}_i^b)^T \mathbf{K} \mathbf{J}_{Ai}^b(\boldsymbol{\theta}_i) \dot{\boldsymbol{\theta}}_i \quad (4.11)$$

The leg of 6LR has 3 degrees of freedom but it has four joints. Therefore, this is a redundant manipulator case. The redundancy can be used for other additional constraint of joint configuration. An objective function of the joint variables  $\omega(\boldsymbol{\theta}_i)$  can be chosen as follows [39]:

$$\omega(\boldsymbol{\theta}_i) = -\frac{1}{2} \theta_{3i}^2 \quad (4.12)$$

The additional vector  $\dot{\mathbf{q}}_{0i}$  for the constraint of joint configuration is defined as

$$\dot{\mathbf{q}}_{0i} = k_0 \left( \frac{\partial \omega(\boldsymbol{\theta}_i)}{\partial \boldsymbol{\theta}_i} \right)^T \quad (4.13)$$

where  $k_0 > 0$ .

From Eqs. (4.12) and (4.13),  $\dot{\mathbf{q}}_{0i}$  can be rewritten as

$$\dot{\mathbf{q}}_{0i} = k_0 [0 \quad 0 \quad -\theta_{3i} \quad 0]^T \quad (4.14)$$

A control input vector is chosen as angular joint velocity vector of leg  $i$  as follows:

$$\dot{\boldsymbol{\theta}}_i = (\mathbf{J}_{Ai}^b)^T (\boldsymbol{\theta}_i) \mathbf{K} \mathbf{e}_i^b + \left( \mathbf{I}_n - (\mathbf{J}_{Ai}^b)^+ \mathbf{J}_{Ai}^b \right) \dot{\mathbf{q}}_{0i} \quad (4.15)$$

where  $(\mathbf{J}_{Ai}^b)^+$  is right pseudo-inverse of  $\mathbf{J}_{Ai}^b$  as

$$(\mathbf{J}_{Ai}^b)^+ = (\mathbf{J}_{Ai}^b)^T \left( \mathbf{J}_{Ai}^b (\mathbf{J}_{Ai}^b)^T \right)^{-1} \quad (4.16)$$

Substituting Eq. (4.15) into (4.11) leads to

$$\begin{aligned} \dot{V}_i(\mathbf{e}_i^b) &= (\mathbf{e}_i^b)^T \mathbf{K} \dot{\mathbf{p}}_{di}^b - (\mathbf{e}_i^b)^T \mathbf{K} \mathbf{J}_{Ai}^b (\mathbf{J}_{Ai}^b)^T \mathbf{K} \mathbf{e}_i^b \\ &\quad - (\mathbf{e}_i^b)^T \mathbf{K} \mathbf{J}_{Ai}^b \left( \mathbf{I}_n - (\mathbf{J}_{Ai}^b)^+ \mathbf{J}_{Ai}^b \right) \dot{\mathbf{q}}_0 \\ &= (\mathbf{e}_i^b)^T \mathbf{K} \dot{\mathbf{p}}_{di}^b - (\mathbf{e}_i^b)^T \mathbf{K} \mathbf{J}_{Ai}^b (\mathbf{J}_{Ai}^b)^T \mathbf{K} \mathbf{e}_i^b \\ &\quad - (\mathbf{e}_i^b)^T \mathbf{K} \left( (\mathbf{J}_{Ai}^b) - (\mathbf{J}_{Ai}^b) (\mathbf{J}_{Ai}^b)^+ \mathbf{J}_{Ai}^b \right) \dot{\mathbf{q}}_0 \\ &= (\mathbf{e}_i^b)^T \mathbf{K} \dot{\mathbf{p}}_{di}^b - (\mathbf{e}_i^b)^T \mathbf{K} \mathbf{J}_{Ai}^b (\mathbf{J}_{Ai}^b)^T \mathbf{K} \mathbf{e}_i^b \\ &\quad - (\mathbf{e}_i^b)^T \mathbf{K} \left( \mathbf{J}_{Ai}^b - \mathbf{J}_{Ai}^b \right) \dot{\mathbf{q}}_0 \end{aligned} \quad (4.17)$$

If  $\mathbf{p}_{di}^b$  is constant, because the third term of Eq. (4.17) is zero, Eq. (4.11) is negative definite as follows:

$$\begin{aligned}\dot{V}_i(\mathbf{e}_i^b) &= -(\mathbf{e}_i^b)^T \mathbf{K} \mathbf{J}_{Ai}^b (\mathbf{J}_{Ai}^b)^T \mathbf{K} \mathbf{e}_i^b \\ &= -\left[ (\mathbf{J}_{Ai}^b)^T \mathbf{K} \mathbf{e}_i^b \right]^T (\mathbf{J}_{Ai}^b)^T \mathbf{K} \mathbf{e}_i^b < 0\end{aligned}\quad (4.18)$$

The condition  $\dot{V}_i < 0$  and  $V_i > 0$  implies that  $\mathbf{e}_i^b = 0$  when time  $t \rightarrow \infty$ , i.e., the system is asymptotically stable.

The matrix  $\mathbf{I}_n - (\mathbf{J}_{Ai}^b)^+ \mathbf{J}_{Ai}^b$  in Eq. (4.15) allows the projection of the vector  $\dot{\mathbf{q}}_0$  in the null space of  $\mathbf{J}_{Ai}^b$ , so that the condition (4.18) is not violated. It means that internal motions described by  $(\mathbf{I}_n - (\mathbf{J}_{Ai}^b)^+ \mathbf{J}_{Ai}^b) \dot{\mathbf{q}}_0$  can reconfigure the leg structure without changing the end effector position and orientation. The chosen controller of Eq. (4.15) makes the end effector be in a desired position.

The joint angles are used to control the servomotors. The joint angles can be calculated in discrete time by the Euler integration method. With sampling time  $\Delta t$ , if the joint angles and angular velocities at time  $t_k$  are known, the joint angles at time  $t_{k+1} = t_k + \Delta t$  can be computed as follows:

$$\boldsymbol{\theta}_i^{t_{k+1}} = \boldsymbol{\theta}_i^{t_k} + \dot{\boldsymbol{\theta}}_i^{t_k} \Delta t \quad (4.19)$$

Fig. 4.13 shows the block diagram of walking controller as follows:

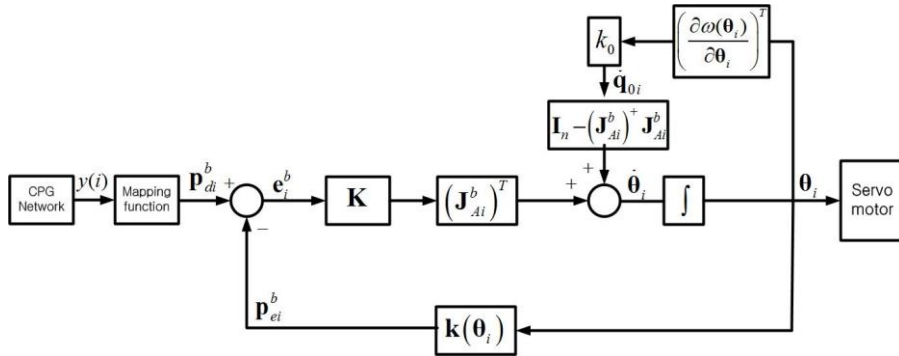


Fig. 4.13 Block diagram of workspace trajectory tracking controller



## Chapter 5: Simulation and Experimental Results

This chapter shows the simulation and experimental results of the proposed gait planning algorithm based on CPG network and trajectory tracking algorithm for a leg based on differential kinematics.

### 5.1 Gait planning simulation results

The parameters and initial values for the simulation of CPG network are listed in Table 5.1

Table 5.1 Values of the parameters of the CPG network

Parameters	Values
$\tau, \tau'$	0.04, 0.6
$u_0$	2
$w_{fe}$	2
$\beta$	5
$feed_{\{e,f\}i}$	0
$\begin{bmatrix} u_{e1} & v_{e1} & u_{f1} & v_{f1} \\ u_{e2} & v_{e2} & u_{f2} & v_{f2} \\ u_{e3} & v_{e3} & u_{f3} & v_{f3} \\ u_{e4} & v_{e4} & u_{f4} & v_{f4} \\ u_{e5} & v_{e5} & u_{f5} & v_{f5} \\ u_{e5} & v_{e5} & u_{f5} & v_{f5} \end{bmatrix}$	$\begin{bmatrix} 0.0139 & 0.0243 & 0.0211 & 0.0026 \\ 0.0265 & 0.0049 & 0.0167 & 0.0130 \\ 0.0132 & 0.0115 & 0.0135 & 0.0107 \\ 0.0236 & 0.0153 & 0.0131 & 0.0089 \\ 0.0090 & 0.0021 & 0.0134 & 0.0022 \\ 0.0272 & 0.0003 & 0.0206 & 0.0057 \end{bmatrix}$

The connecting weight matrix of wave gait, quadruped gait and tripod gait are shown as follows:

$$W_{wg} = \begin{bmatrix} 0 & -1 & -1 & -1 & -1 & -1 \\ -1 & 0 & -1 & -1 & -1 & -1 \\ -1 & -1 & 0 & -1 & -1 & -1 \\ -1 & -1 & -1 & 0 & -1 & -1 \\ -1 & -1 & -1 & -1 & 0 & -1 \\ -1 & -1 & -1 & -1 & -1 & 0 \end{bmatrix} \quad (5.1)$$

$$W_{qg} = \begin{bmatrix} 0 & -1 & -1 & -1 & 1 & -1 \\ -1 & 0 & -1 & -1 & -1 & 1 \\ -1 & -1 & 0 & 1 & -1 & -1 \\ -1 & -1 & 1 & 0 & -1 & -1 \\ 1 & -1 & -1 & -1 & 0 & -1 \\ -1 & 1 & -1 & -1 & -1 & 0 \end{bmatrix} \quad (5.2)$$

$$W_{tg} = \begin{bmatrix} 0 & -1 & 1 & -1 & 1 & -1 \\ -1 & 0 & -1 & 1 & -1 & 1 \\ 1 & -1 & 0 & -1 & 1 & -1 \\ -1 & 1 & -1 & 0 & -1 & 1 \\ 1 & -1 & 1 & -1 & 0 & -1 \\ -1 & 1 & -1 & 1 & -1 & 0 \end{bmatrix} \quad (5.3)$$

In this thesis, periodic gait is chosen for the six legs. Periodic gait means that the step cycle is same for the six legs. There exist several periodic gaits depending on the duty factor and the phase shift between legs such as wave gait, quadruped gait and tripod gait.

### 5.1.1 Wave gait

Fig. 5.1 shows the output signal of CPG network for wave gait. In Fig. 5.1, every leg has different phase position, and they also have same phase difference one by one leg. The sequence of leg in the

swing phase is shown as follows:  $L1 \rightarrow R3 \rightarrow L2 \rightarrow L3 \rightarrow R2 \rightarrow R1$ .  
 The duty factor of the proposed wave gait is  $5/6$ .

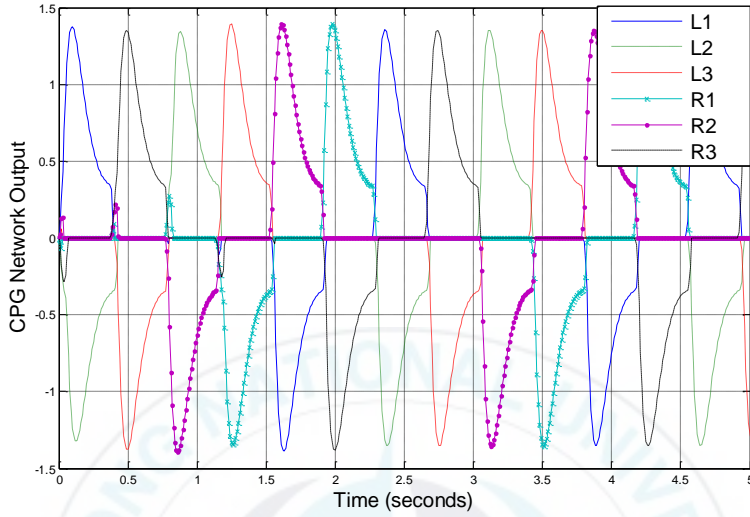


Fig. 5.1 Output of CPG network for wave gait

### 5.1.2 Quadruped gait

Fig. 5.2 shows the output signal of CPG network for quadruped gait. In Fig. 5.2, L1 and R2, L2 and R3, L3 and R1 are in same phase each other. The duty factor of the proposed quadruped gait is  $2/3$ .

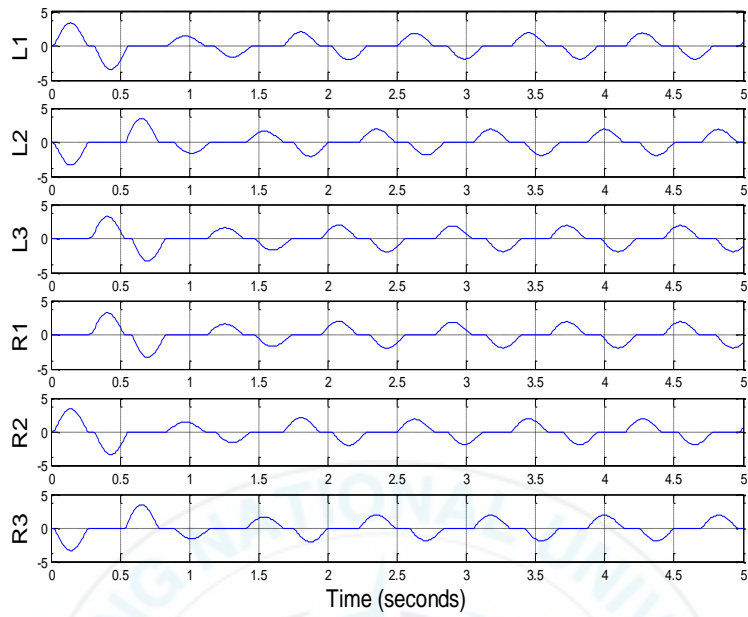


Fig. 5.2 Output of CPG network for quadruped gait

### 5.1.3 Tripod gait

Fig. 5.3 shows the output signals of CPG network for tripod gait. In Fig. 5.3, L1, L3 and R2 are in same phase, and L2, R1 and R3 are in same phase. The duty factor of the proposed tripod gait is 1/2.

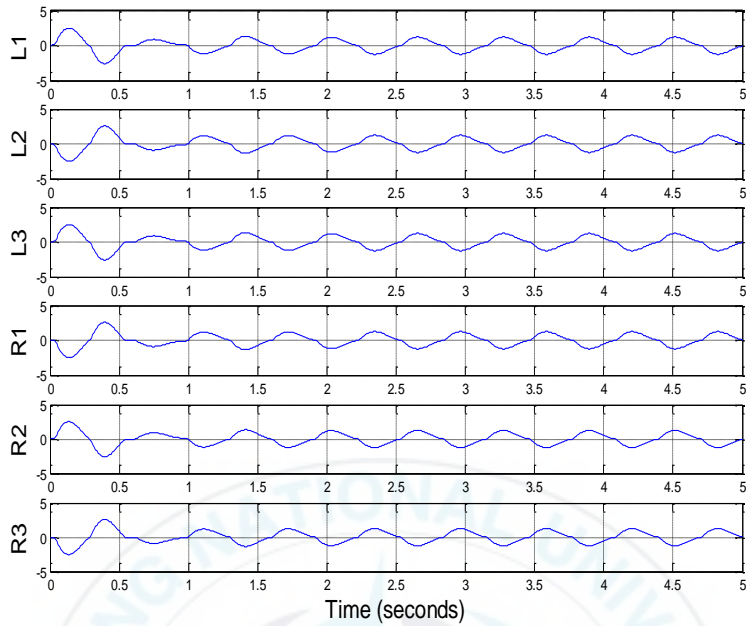


Fig. 5.3 Output of CPG network for tripod gait

## 5.2 Mapping function of tripod gait simulation results

In this thesis, only the simulation results of mapping function for tripod gait are shown. The parameters used for the simulation are listed in Table 5.2.

Table 5.2 Parameters used for the simulation

Parameters	Values	Unit
$\beta$	0	rad
$k_z$	0.05	
$r$	70	mm

Fig. 5.4 shows one of tripod gait signals generated by CPG network. From Fig. 5.4, the time of one cycle is 2 seconds. For tripod gait, the swing phase is 1 second, and the retract phase is 1 second. Fig. 5.5 shows the end effector transformed trajectory of  $x$  axis. The attitude is increased in swing phase and keeps constant in the retract phase. Fig. 5.6 shows the end effector transformed trajectory of  $z$  axis. Because  $\beta = 0$ , the end effector transformed trajectory of  $x$  axis is 0 always.

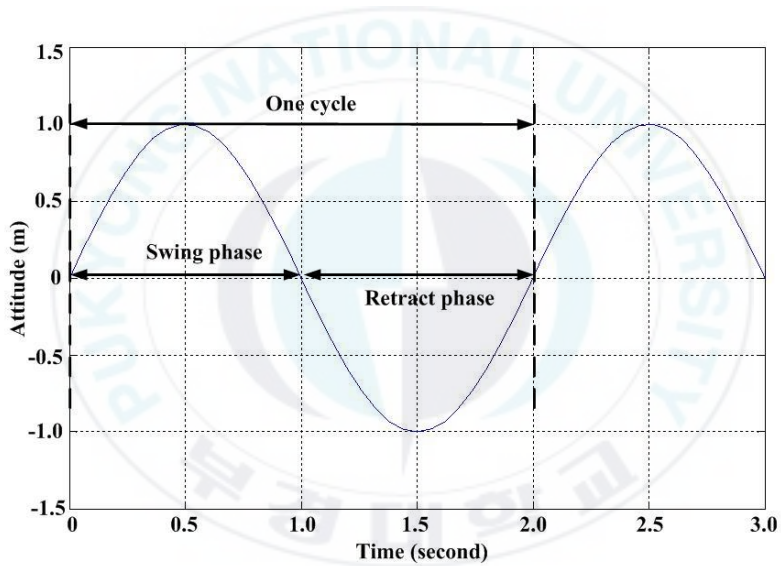


Fig. 5.4 One cycle of CPG network output for tripod gait

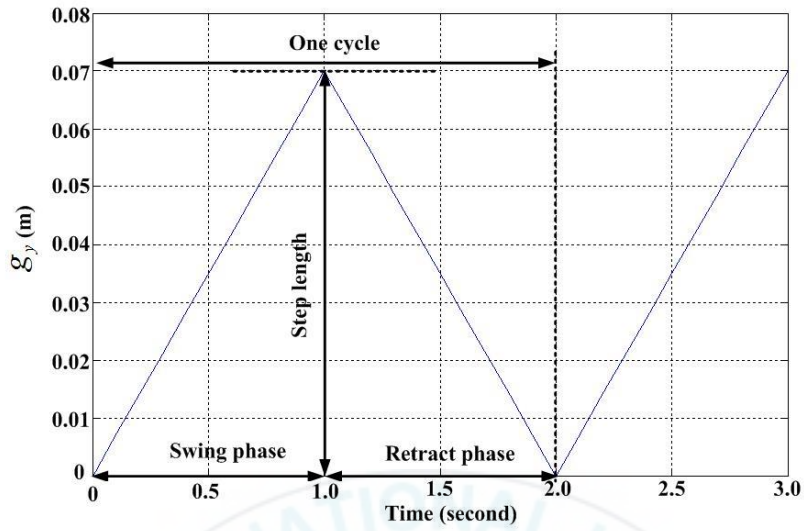


Fig. 5.5 Transformed trajectory for y axis

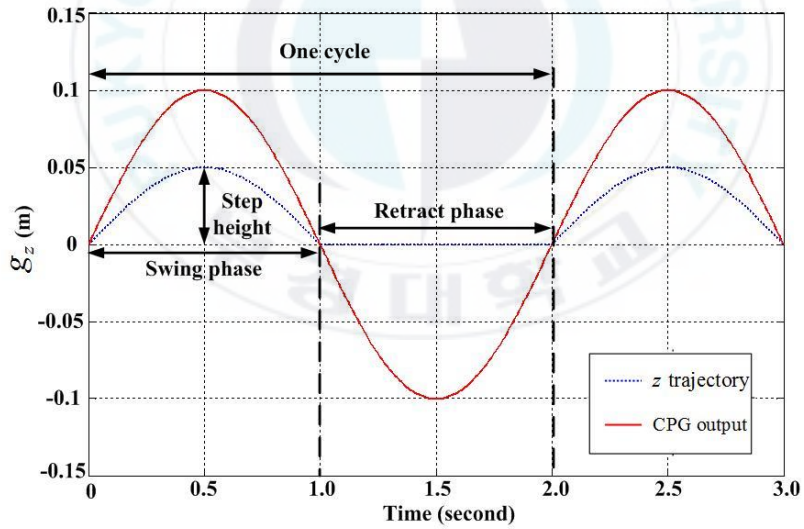


Fig. 5.6 Transformed trajectory for z axis

### 5.3 Workspace trajectory tracking

In this thesis, the simulation results of one leg of the proposed six legged robot are shown to prove the effectiveness and applicability of the proposed controller. The parameters and initial values used for the simulation are listed in Table 5.2 and Table 5.3

Table 5.3 Parameters used for the simulation

Parameters	Values	Unit
$a_1$	67	mm
$a_2$	60.5	mm
$a_3$	22.5	mm
$a_4$	112.7	mm
$d_3$	62	mm

Table 5.4 Initial values used for the simulation

Parameters	Values	Unit
$\theta_1$	0	rad
$\theta_2$	$-\pi / 2$	rad
$\theta_3$	0	rad
$\theta_4$	0	rad
$x_{e0}$	0.129	mm
$y_{e0}$	0	mm
$z_{e0}$	-0.188	mm

Fig. 5.7 shows the leg at the stand position in the initial state. The end effector of the leg stays at  $p_{e0} = [x_{e0}, y_{e0}, z_{e0}]^T$ . After the output of CPG network is mapped, the desired points are computed

and the end effector trajectory is generated. The algorithm is applied for the leg end effector to follow the trajectory to the desired point.

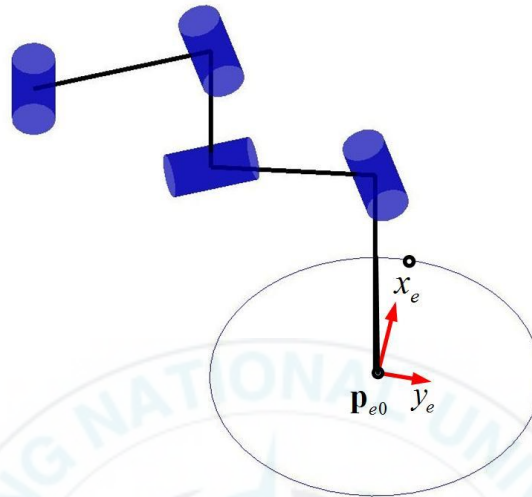


Fig. 5.7 The end effector of one leg at stand position

Fig. 5.8 shows error values of the end effector position vector for one walking cycle time. After 0.3 second, the errors converge to zero from initial errors since the end effector reaches  $P_{d1}$  with lifting up state of swing phase. From 0.5 second to 1 second, the errors are increased for the end effector to reach  $P_{d2}$  and converge to zero rapidly. And then, the end effector puts down and reaches  $P_{d2}$  at 1 second. From 1 second to 2 seconds, the end effector in the retract phase and tracks the trajectory from  $P_{d2}$  to  $P_{d0}$  and the errors are bounded within  $\pm 0.5\text{mm}$ .

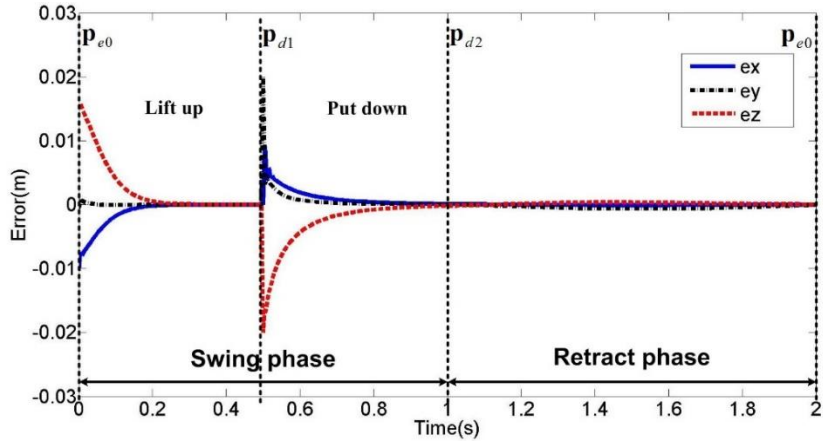


Fig. 5.8 Tracking errors of the end effector of one leg for one walking cycle time

Fig. 5.9 shows the simulation results and experimental results of joint angular velocities of one leg of the 6LR for one walking cycle. From Fig. 5.10, the angular velocities are smooth in swing phase after 1 second. In retract phase, the angular velocities of joints 4 and 2 change sharply since the end effector is tracking the trajectory. The desired positions are closely in this phase.

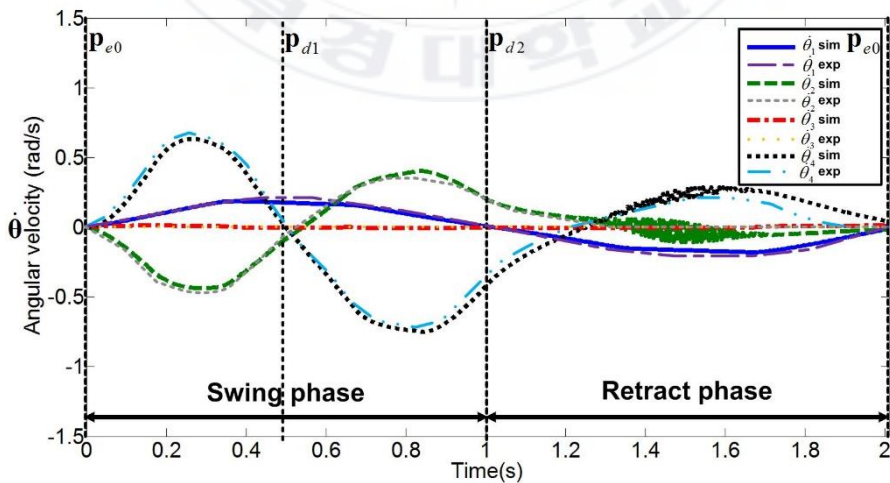


Fig. 5.9 Joint angular velocities of one leg of the 6LR for one walking cycle time

Fig. 5.10 shows the simulation and experimental results of angle of each joint of one leg for one walking cycle time. The angles of the joints are smooth, and the angle of joint 3 is zero since the objective function  $\omega(\mathbf{q})$  is applied. From Fig. 5.10, the experimental results of four joint angles are similar with simulation results.

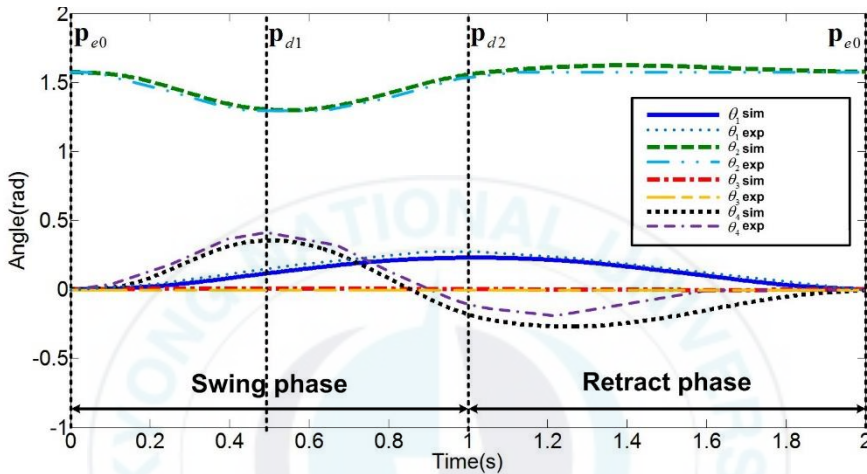


Fig. 5.10 Joint angles of one leg of the 6LR for one walking cycle time

Fig. 5.11 shows the trajectory of the end effector of one leg for one walking cycle time. Leg movement has two states: swing phase and retract phase. In lift up state, the end effector of the leg moves from stand position  $P_{e0}$  in (a) to lift up position  $P_{d1}$  in (b) and then contacts ground position  $P_{d2}$  in (c). In retract phase state, the end effector tracks the trajectory from  $P_{d2}$  to  $P_{e0}$  shown as dotted line in (d).

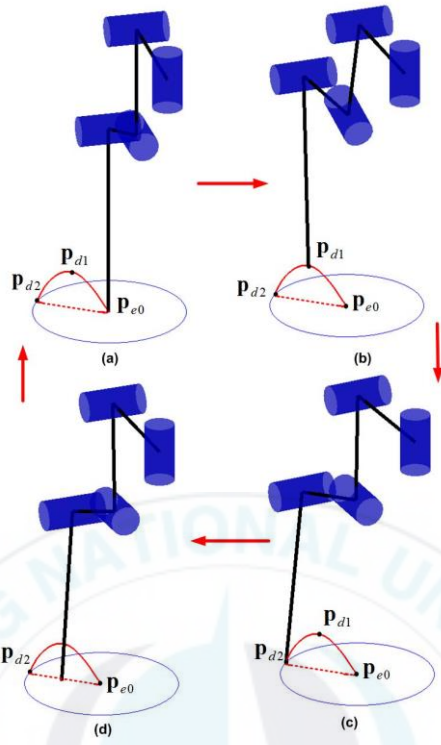


Fig. 5.11 Trajectory of the end effector of one leg for one walking cycle time

# Chapter 6: Conclusions and Future Work

## 6.1 Conclusions

This thesis is about a locomotion control of six-legged robot based on central pattern generator network. The conclusions of this thesis are summarized as follows:

- The description of a six-legged robot and its hardware configuration were presented, and the typical definitions for the six-legged robot and the stability of walking gait were stated. The kinematic modeling of one leg of the six-legged robot was presented based on D-H convention.
- A CPG model based on Kimura's neural oscillator model was introduced which corresponded to flexor neural and extensor neuron, respectively. The parameters analysis of the CPG model was presented.
- A CPG network to generate three kinds of gait for the six-legged walking robot such as wave gait, quadruped gait and tripod gait was built. Six coupled oscillators were used to denote the CPG network, and each oscillator was used to control one leg by generate phase signal. Mapping functions were designed to map the phase signals generated by CPG network into the workspace trajectory of the corresponding end effector of legs.
- A workspace trajectory tracking controller was designed to control the leg end effector of one leg to track the trajectory generated by mapped the output signal of CPG network based on differential kinematics algorithm.

- Simulations and experiments were conducted to verify the effectiveness and performances of the mathematical modeling and the designed controllers. For gait planning, wave gait, quadruped gait and tripod gait were generated by using different connecting weight matrix based on CPG network. The output signal of tripod gait generated by CPG network was transformed to workspace trajectory of the end effector by the designed mapping function. In the workspace trajectory tracking case, instead of inverse kinematics, the differential kinematics algorithm was used to obtain the joint angle of each leg.
- The simulation results of tracking error of the end effector were presented. The error converged to zero from initial errors after 0.3 second. From 0.5 second to 1 second, the errors were increased for the end effector to reach  $p_{d2}$  and converged to zero rapidly. From 1 second to 2 seconds, the end effector tracked the trajectory from  $p_{d2}$  to  $p_{e0}$  and the error were bounded within  $\pm 0.5\text{mm}$ .
- The simulation and experimental results of joint angles of one leg were presented. The angles of joints were smooth. From 0 to 1 second, the leg was in the swing phase. Joint 1 has increased 0.25rad, and joint 2 has increased 0.2 rad in negative direction in the 0.5 seconds then moved back initial position in the last 0.5 seconds, and joint 4 increased 0.4rad in the 0.5 seconds and moved to initial position after 0.4 seconds. From 1 second to 2 second, the leg was in the retract phase. Joint 1 and joint 4 have moved to initial position in 1 seconds, and joint 2 kept constant angle. The angle of joint3 was zero both in swing phase and

retract phase. The end effector followed the trajectory successfully and the angle of each joint was obtained.

## **6.2 Future work**

This thesis presented a locomotion control of a six-legged walking robot based on central pattern generator network. However, the modification and development for upgrading and extending the system can be done totally. There are some ideas that will be considered as future works:

- Because the CPG equation has nonlinearity, coupling and higher-dimension, it is difficult to master dynamics of CPG equation. By tuning the parameters of CPG model, the gait transition behavior of the six-legged robot should be considered.
- The proposed controller considered only kinematic modeling. Since our robot uses servomotors, it is difficult to apply a dynamic modeling and a dynamic controller. The dynamic modeling of the 6LR should be stated to improve the control performance. With dynamic modeling, the mass of the robot, the reaction force on each leg and other parameters can be considered to design a better controller for the robot.
- The simulations and experiments were performed on the flat terrain and the rough terrain condition is not considered. However, the walking controller design of the 6LR on rough terrain can be an interesting topic for future work.

## References

- [1] D. J. Todd, “*Walking Machines: An Introduction to Legged Robots*,” Chapman and Hall Advanced Industrial Technology Series, Springer US, pp. 11-21, 1985.
- [2] K. J. Waldron, V. J. Vohnout, A. Pery and R. B. McGhe, “*The Adaptive Suspension Vehicle*,” The International Journal of Robotics Research, Vol. 3, No. 3, pp. 31-36, 1984.
- [3] R. Brooks, “*A Robot that Walks; Emergent Behaviors From a Carefully Evolved Network*,” Neural Computation, Vol. 1, No. 2, pp. 253-262, 1989.
- [4] C. Angle and R. Brooks, “*Small Planetary Rovers*,” Proceedings of IEEE International Workshop on Intelligent Robots and Systems’90, pp. 383-388, 1999.
- [5] M. Raibert, K. Blankespoor, G. Nelson, R. Playter and T. B. Team, “*Bigdog, the Rough-Terrain Quadruped Robot*,” In Proceeding of the 17<sup>th</sup> World Congress, Vol. 17, No. 1, pp. 10822-10825, 2008.
- [6] J. Y. Kim and B. H. Jun, “*Design of Six-Legged Walking Robot, Little Crabster for Underwater Walking and Operation*,” Advanced Robotics, Vol. 28, No. 2, pp. 77-89, 2014.
- [7] M. L. Shik, F. V. Severin and G. N. Orlovsky, “*Control of Walking and Running by Means of Electrical Stimulation of Mid-brain*,” Electroencephalography and Clinical Neurophysiology, Vol. 26, No. 5, pp. 549, 1969.
- [8] B. Webb and T. R. Consi, “*Biorobotics: Methods and Applications*,” MIT Press, 2001.

- [9] J. Ayers, J. L. Davis and A. Rudolf, “*Neurotechnology for Biomimetic Robots*,” MIT Press, 2002
- [10] S. L. Hooper, “*Central Pattern Generators*,” *Current biology: CB*, Vol. 10, No. 5, pp. 176, 2000.
- [11] F. Delcomyn, “*Neural Basis for Rhythmic Behavior in Animals*,” *Science*, Vol. 210, No. 4469, pp.492-498, 1980.
- [12] I. Delvolvé, P. Branchereau, R. Dubuc and J. M. Cabelguen, “*Fictive Rhythmic Motor Patterns Induced by NMDA in an In Vitro Brain Stem-spinal Cord Preparation from an Adult Urodele*,” *Journal of Neurophysiology*, Vol. 82, No. 2, pp. 1074-1077, 1999.
- [13] A. H. Cohen, P. Holmes and R. Rand, “*The Nature of Coupling between Segmented Oscillations and the Lamprey Spinal Generator for Locomotion: A Mathematical Model*,” *Journal of Mathematical Biology*, Vol. 13, No. 3, pp. 345-369, 1982.
- [14] K. Matsuoka, “*Sustained Oscillations Generated by Mutually Inhibiting Neurons with Adaptation*,” *Biological Cybernetics*, Vol. 52, No. 6, pp. 367-376, 1985.
- [15] S. T. Venkataraman, “*A Simple Legged Locomotion Gait Model*,” *Robotics and Autonomous Systems*, Vol. 22, No. 1, pp. 75-85, 1997.
- [16] G. Taga, “*A Model of the Neuro-Musculo-Skeletal System for Human Locomotion*,” *Biological cybernetics*, Vol. 73, No. 2, pp. 97-111, 1995.
- [17] A. Billard and A. J. Ijspeert, “*Biologically Inspired Neural Controllers for Motor Control in a Quadruped Robot*,” *Neural Networks*, 2000. IJCNN 2000, Proceeding of the IEEE-ENNS

- International Joint Conference on Neural Networks, Vol. 6, pp. 637-641, 2000.
- [18] H. Kimura, S. Akiyama and K. Sakurama, “*Realization of Dynamic Walking and Running of the Quadruped Using Neuron Oscillator*”, *Autonomous Robots*, Vol. 7, No. 3, pp. 247-258, 1999.
- [19] H. Kimura and Y. Fukuoka, “*Adaptive Dynamic Walking of a Quadruped Robot on Irregular Terrain by Using Neural System Model*”, *Proceedings of the 2000 IEEE/RSJ International Conference on Intelligent Robot and Systems*, Vol. 2, pp. 979-984, 2000.
- [20] S. Inagaki, H. Yuasa and T. Arai, “*CPG Model for Autonomous Decentralized Multi-Legged Robot System—Generation and Transition of Oscillation Patterns and Dynamics of Oscillators*,” *Robotics and Autonomous System*, Vol. 44, No. 3, pp. 171-179, 2003.
- [21] P. Manoonpong, F. Pasemann and F. Wörgötter, “*Sensor-Driven Neural Control for Omnidirectional Locomotion and Versatile Reactive Behaviors of Walking Machines*,” *Robotics and Autonomous Systems*, Vol. 56, No. 3, pp. 265-288, 2008.
- [22] A. J. Ijspeert, A. Crespi, D. Rycko and J. M. Cabelguen, “*From Swimming to Walking with a Salamander Robot Driven by a Spinal Cord Model*,” *Science*, Vol. 315, No. 5817, pp. 1416-1420, 2007.
- [23] A. J. Ijspeert, “*A Connectionist Central Pattern Generator for the Aquatic and Terrestrial Gaits of a Simulated Salamander*,” *Biological cybernetics*, Vol. 84, No. 5, pp. 331-348, 2001.

- [24] A. J. Ijspeert, A. Crespi and J. M. Cabelguen, “*Simulation and Robotics Studies of Salamander Locomotion,*” *Neuroninformatics*, Vol. 3, No. 3, pp. 171-195, 2005.
- [25] A. Crespi and A. J. Ijspeert, “*Online Optimization of Swimming and Crawling in an Amphibious Snake Robot,*” *IEEE Transaction on Robotics*, Vol. 24, No. 1, pp. 75-87, 2008.
- [26] S. Inagaki, H. Yuasa and T. Arai, “*CPG Model for Autonomous Decentralized Multi-legged Robot System-Generation and Transition of Oscillation Patterns and Dynamics of Oscillators,*” *Robotics and Autonomous Systems*, Vol. 44, No. 3, pp. 171-179, 2003.
- [27] S. Inagaki, H. Yuasa, T. Suzuki and T. Arai, “*Wave CPG Model for Autonomous Decentralized Multi-legged Robot: Gait Generation and Walking Speed Control,*” *Robotics and Autonomous System*, Vol. 54, No. 2, pp. 118-126, 2006.
- [28] K. Tsuchiya, K. Tsujita, K. Manabu and S. Aoi, “*An Emergent Control of Gait Patterns of Legged Locomotion Robots,*” *IAV, Intelligent Autonomous Vehicles*, pp. 271-276, 2001.
- [29] K. Tsujita, K. Tsuchiya and A. Onat, “*Adaptive Gait Pattern Control of a Quadruped locomotion Robot,*” *Proceedings of the 2001 IEEE/RSJ International Conference on Intelligent Robots and Systems*, Vol. 4, pp. 2318-2325, 2001.
- [30] G. Endo, J. Nakanishi, J. Morimoto and G. Cheng, “*Experimental Studies of a Neural Oscillator for Biped Locomotion with QRIO,*” *Proceedings of the 2005 IEEE International Conference on Robotics and Automation*, pp. 596-602, 2005.

- [31] K. Matsuoka, “*Mechanisms of Frequency and Pattern Control in the Neural Rhythm Generators*,” *Biological Cybernetics*, Vol. 56, pp. 245-353, 1987.
- [32] M. M. Williamson, “*Design Rhythmic Motion Using Neural Oscillators*,” *Proceedings of the 1999 IEEE/RSJ International Conference on Intelligent Robots and Systems*, Vol. 1, pp. 494-500, 1999.
- [33] J. H. Jianjue, M. M. Williamson and A. P. Gill, “*Bipedal Locomotion Control with Rhythmic Neural Oscillators*,” *Proceedings of the 1999 IEEE/RSJ International Conference on Intelligent Robots and Systems*, Vol. 3, pp. 1475-1481, 1999.
- [34] A. M. Arsenio, “*Tuning of Neural Oscillators for the Design of Rhythmic Motions*,” *Proceedings of the ICRA '00 IEEE International Conference on Robotics and Automation*, Vol. 2 pp. 1888-1893, 2000.
- [35] H. Yuasa and M. Ito, “*Coordination of Many Oscillators and Generation of Locomotion Patterns*,” *Biological Cybernetics*, pp. 177-184, 1990.
- [36] G. Taga, “*A Model of the Neuro-Musculo-Skeletal System for Human Locomotion*,” *Biological Cybernetics*, Vol. 73, No. 5, pp. 113-121, 1995.
- [37] S. Ok, K. Miyashita and K. Hase, “*Evolving Bipedal Locomotion with Genetic Programming – A Preliminary Report*,” *Proceedings of the 2001 Congress on Evolutionary Computation*, Vol. 2, pp. 1025-1032, 2001.
- [38] S. Jiang, J. S. Cheng and J. P. Chen, “*Design of Central Pattern Generator for Humanoid Robot Walking Based on Multi-Objective GA*”, *Proceedings of the 2000 IEEE/RSJ*

International Conference on Intelligent Robot and Systems, Vol. 3, pp. 1930-1935, 2000.

- [39] B. Siciliano, L. Sciavicco, L. Villani and G. Oriolo, “*Robotics: Modeling, Planning and Control,*” Springer-Verlag, 2009.



# Publications and Conferences

## A. Publications

1. **Dong Bo Sheng**, Hung Nguyen Huy, Pandu Sandi Pratama, Hak Kyeong Kim, Vo Hoang Duy and Sang Bong Kim, “*Walking Gait Planning Using Central Pattern Generators for Hexapod Walking Robot*”, Lecture Notes in Electrical Engineering, pp: 671-684, 2015. SCOPUS

## B. Conferences

1. **Sheng Dongbo**, Trong Hai Nguyen, Tian Shui Gao, Hak Kyeong Kim and Sang Bong Kim, “*Measurement of Injured Rate of Fish Surface Using Image Segmentation*”, KSME Dynamic Engineering and Control Division Spring Conference, The Korean Society of Mechanical Engineers, Buyeo, Korea, 2016.
2. **D. B. Sheng**, S. B. Kim, D. Dhayfole, T. S. Gao and H. K. Kim, “*Analysis of Injured Rate Using Color Image Segmentation Based on K-means Clustering Algorithm*”, KSPE 2016 Spring Conference, The Korean Society for Precision Engineering, Jeju, Korea, 2016.
3. A. V. Gulalkari, **D. B. Sheng**, P. S. Pratama, H. K. Kyeong, G. S. Byun and S. B. Kim, “*Kinect Camera Sensor-Based Object Tracking and Following of Four Wheel Independent Steering Automatic Guided Vehicle Using Kalman Filter*”, 2015 15<sup>th</sup>

International Conference on Control, Automation and Systems (ICCAS 2015), Bexco, Korea, 2015.

4. Pandu Sandi Pratama, Jin-Wook Kim, **Dong-Bo Sheng**, Suk-Min Yoon, Tae-Kyeong Yeu, Sup Hong, Hak-Kyeong Kim and Sang-Bong Kim, “*Comparison of Optimization Methods to Minimize the Overlapped Path in Coverage Path Planning for Underwater Mining Robot*”, KSOE Fall Conference, The Korean Society of Ocean Engineers, Daejeon, Korea, 2015.



# Appendix A

Denavit-Hartenberg (DH) convention can be described as follows:

- Choose axis  $z_i$  along the axis of joint  $i + 1$ .
- Locate the origin  $O_i$  at the intersection of axis  $z_i$  with the common normal to axes  $z_{i-1}$  and  $z_i$ . Also, locate  $O_{i'}$  at the intersection of the common normal with axis  $z_{i-1}$ .
- Choose axis  $x_i$  along the common normal to axes  $z_{i-1}$  and  $z_i$  with direction from joint  $i$  to joint  $i + 1$ .
- Choose axis  $y_i$  so as to complete a right-handed frame.

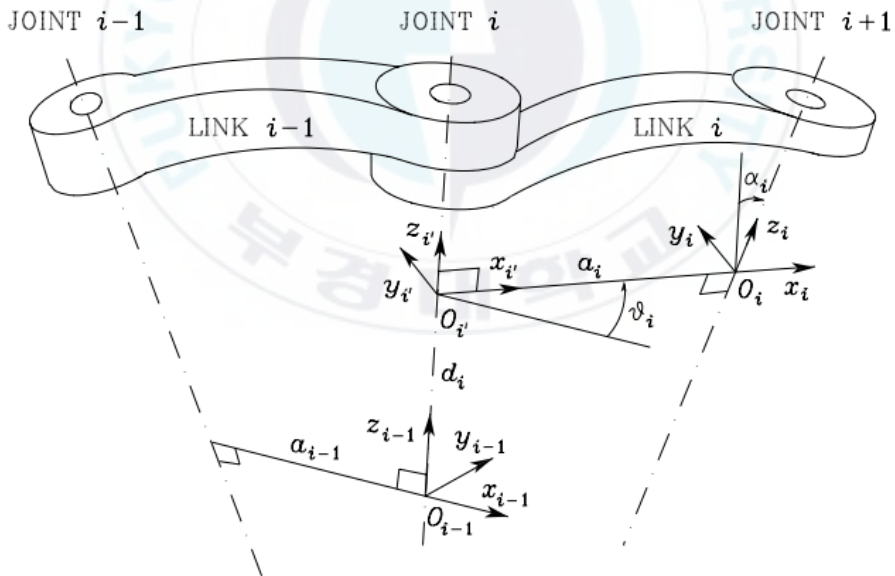


Fig. A.1 Denavit-Hartenberg kinematic parameters

Once the link frames have been established as shown in Fig. A.1, the position and orientation of frame  $i$  with respect to frame  $i - 1$  are completely specified by the following parameters:

$a_i$  : Distance between  $O_i$  and  $O_{i'}$

$d_i$  : Coordinate of  $O_{i'}$  along  $z_{i-1}$

$\alpha_i$  : Angle between axes  $z_{i-1}$  and  $z_i$  about axis  $x_i$  to be taken positive when rotation is made counter-clockwise

$\theta_i$  : Angle between axes  $x_{i-1}$  and  $x_i$  about axis  $z_{i-1}$  to be taken positive when rotation is made counter-clockwise.



E.O.D.